

RESEARCH ARTICLE

10.1029/2019JC015282

Key Points:

- Freshwater residence time in Lake Pontchartrain is 25 days; Wind controls salt content and residence time inside the System
- increasing wind magnitude enhances both surface downwind flow and bottom upwind flow and lower the no-motion surface between opposing flows
- leakage of freshwater through the diversion prior to its official opening has been proven to be significant for salinity inside the estuary

Correspondence to:

C. Li,
cli@lsu.edu

Citation:



Huang, W., Li, C., White, J. R., Bargu, S., Milan, B., & Bentley, S. (2020). Numerical experiments on variation of freshwater plume and leakage effect from Mississippi River diversion in the Lake Pontchartrain Estuary. *Journal of Geophysical Research: Oceans*, 125, e2019JC015282. <https://doi.org/10.1029/2019JC015282>

Received 11 MAY 2019

Accepted 14 JAN 2020

Accepted article online 7 JAN 2020

Numerical Experiments on Variation of Freshwater Plume and Leakage Effect From Mississippi River Diversion in the Lake Pontchartrain Estuary

Wei Huang¹ , Chunyan Li^{1,2} , John R. White^{1,2}, Sibel Bargu¹, Brian Milan¹, and Sam Bentley^{2,3}

¹Department of Oceanography and Coastal Sciences, College of the Coast and Environment, Louisiana State University, Baton Rouge, LA, USA, ²Coastal Studies Institute, Louisiana State University, Baton Rouge, LA, USA, ³Department of Geology and Geophysics, Louisiana State University, Baton Rouge, LA, USA

Abstract A Finite Volume Community Ocean Model is used to investigate how wind impacts the circulation and evolution of a freshwater plume from Mississippi River diversion in the Lake Pontchartrain Estuary. Results show that northerly and southerly winds tend to stretch the plume in the east-west directions, while easterly and westerly winds constrain the plume in the north-south directions. Increasing wind magnitude tends to increase the total salt content of the estuary except under weak westerly wind (<6 m/s) during which salt content decreases. A no-motion middepth interface is found (by the model and verified by the data), separating the top layer downwind flow and bottom layer upwind flow. Increasing wind magnitude can enhance the two-layered flows and lower the no-motion plane between the two opposite flows. Apparent small leakage of the river water through the diversion structure prior to its opening is found to impact the vertical structure of flows and salinity: Mixing is facilitated by the large amount of freshwater leaked into the lake prior to the opening of the diversion; wind-driven gyres are diminished; the average potential energy demand, a quantity used to measure the vertical stratification, is reduced to very low values; more deviation from the quasi-steady state balance tends to occur; and a total of 3.7×10^8 kg of salt is reduced during the opening period of the Bonnet Carré Spillway. The Lake Pontchartrain Estuary is completely dominated by the river water within about 25 days, when salinity drops from an average value of 4 g/kg to essentially zero.

1. Introduction

1.1. River Plumes

Coastal plumes are common both inside and outside of estuaries. A surface plume is usually a region of buoyant water with a sharp dynamic boundary (the front) with the ambient water. The plume spreads horizontally under gravity over the heavier and more saline ambient water (Garvine, 1977, 1987; Kourafalou et al., 1996), while mixing occurs at the front. The plume region is characterized by enhanced stability, increased density gradient, and convergence at the front (Garvine & Monk, 1974; O'Donnell et al., 1998; O'Donnell et al., 2008). The plume caused by the discharge of river water into coastal region has a significant impact on suspended sediment transport (Dinnel et al., 1990), dispersion of pollutants (DiGiacomo et al., 2004; Eisma, 1981), plankton communities (Chen et al., 2009; Lehrter et al., 2009), bacterial concentrations (Ackerman & Weisberg, 2003), water quality (Araújo et al., 2017), geo-chemical characteristics (Nezlin et al., 2008), and even air-sea interactions (Huang et al., 2013).

Freshwater plumes are affected by a variety of factors including coastal currents, tides, bathymetry, river discharge, and Earth rotation (Horner-Devine et al., 2009; Lee & Valle-Levinson, 2013; Marsaleix et al., 1998; Oey & Mellor, 1993; Ou et al., 2009; Shi & Wang, 2009; Wiseman & Garvine, 1995; Zu & Gan, 2015). For example, Halverson and Pawlowicz (2008) reported that the salinity in a plume is a quasi-linear function of river discharge. The study also demonstrated that the salinity of the plume varies on tidal and fortnightly time scales and decreases the most at the end of large ebbs. On the other hand, when the estuary width is equal to or greater than the Rossby deformation radius, the Coriolis effect cannot be ignored. The effect of Earth rotation will lead to a laterally asymmetric plume and a two-layered circulation (Chao, 1988; Chao & Boicourt, 1986). Furthermore, the Coriolis force sets up a coastal current directing the meandering plume

toward the shore (Garvine, 1987). O'Donnell (1990) discussed how alongshore currents affect the buoyant plume, and the study concluded that a smaller alongshore velocity will facilitate the expansion of buoyant layer with a thinner plume but a larger area of the plume and more susceptible to vertical mixing as demonstrated by Garvine (1984).

Another important factor in controlling the evolution and dynamics of a freshwater plume is wind (Horner-Devine, 2009). Zu et al. (2014) pointed out that wind determines the horizontal shape and spreading of the plume by wind-driven coastal currents. Winds and ambient wind-driven current play important roles in transporting the freshwater downstream (Dong et al., 2004; Fong & Geyer, 2002; Gan et al., 2009; Hordoir et al., 2006). For instance, a study of Merrimack River plume by Kakoulaki et al. (2014) shows that the plumes with scales less than 12 km are sensitive to wind direction when wind speed exceeds 4 m/s. Androulidakis et al. (2015) used a numerical model to examine the role of wind-driven circulation on the evolution of Mississippi River plume into the Gulf of Mexico. They demonstrated that the downstream flow over the Louisiana-Texas shelf can be strengthened by the downwelling-favorable winds, thus deepening the plume. The transport of Mississippi River plume water toward the Mississippi-Alabama-Florida shelf, however, can be enhanced by upwelling-favorable wind as it eliminates or reverses the downstream current. This observation is similar to the findings in the Delaware coastal plume (Jiang et al., 2009). Studies of Hickey et al. (1998) and Berdeal et al. (2002) both confirmed that downwelling/upwelling winds would drive the buoyant plume from Columbia River onshore/offshore. Ekman currents associated with the upwelling favorable winds tend to widen and thin the river plume (Fong & Geyer, 2001; Houghton et al., 2004).

Wind has a great impact on the orientation and development of freshwater or saltwater plumes (Lentz, 1995; van den Huevel, 2010). Walker (1999) and Walker et al. (1996) studied the Mississippi River plume by using satellite images and in situ measurements. They demonstrated that the northeasterly, easterly, and southeasterly winds push the plume waters seaward, and eastward wind-related Ekman transport can enlarge the offshore river plume. Walker et al. (2005) also investigated the relationship between the seasonal variation of wind's direction and the structure of the Mississippi River Plume. The results show that river waters are driven westward by easterly winds in autumn, winter, and spring, leading to the increased river discharge onto the Louisiana-Texas shelf. In addition, the direction of movement of the plume can be reversed by atmospheric cold fronts. Valle-Levinson et al. (2007) explored the impact of bathymetry and local and remote atmospheric effects on the Chesapeake Bay outflow plume. The plume is found to be separated and an inshore front is formed, in addition to the customarily described offshore front. In a study for the Peal River estuary's plume front in winter (Zheng et al., 2014), it was found that both wind speed and wind direction influence the evolution of the plume. Moderate down-estuary winds enhance estuarine stratification, while strong down-estuary winds and all up-estuary winds reduce stratification (Chen & Sanford, 2009; Xie & Li, 2018). Li and Li (Li & Li, 2011, 2012) proposed that the difference between down-estuary and up-estuary wind effects on the stratification and circulation. Both down-estuary and up-estuary winds can decrease the stratification when Coriolis force is not taken into consideration, down-estuary (up-estuary) wind can induce a counterclockwise (clockwise) lateral circulation.

1.2. Plume in the Low-Salinity Estuary—Lake Pontchartrain

The goal of this study was to investigate the river plume from the Mississippi River water diversion into the low-salinity Lake Pontchartrain Estuary (LPE) through the Bonnet Carré Spillway (BCS). We will therefore focus on the review of previous work in this estuary in the following.

Plumes have been observed in the LPE during spring flood season when a manmade diversion structure, the BCS, is opened to relieve downstream flood pressure, hence, reducing risk of flooding to the city of New Orleans, LA. Historically, the spillway had been opened roughly every 10 years and thus the plume occurred as an infrequent event. However, in the past decade alone, an apparent increase of spring river flood events has led to five openings (2008, 2011, 2016, 2018, and 2019). The plume of freshwater diverted into the estuary is unique in that it is within an enclosed, oligohaline estuary with mean salinity of only ~4–5. A total amount of 9.1 million metric tons of sand was deposited on the Mississippi River Channel adjacent to the BCS (Allison et al., 2013) during the opening event in 2011. Georgiou et al. (2009) investigated the salinity distributions with freshwater input from adjacent rivers and BCS under tidal forcing, which indicates a significant reduction in salinity.

The low salinity, low turbidity, and high-nutrient environment are favorable for the formation of harmful cyanobacteria blooms, capable of adversely affecting water resources in the LPE (Bargu et al., 2011; McCorquodale et al., 2009; Roy et al., 2016; White et al., 2009). Recent studies have shown that the LPE experiences high interannual variability in nutrients and phytoplankton community, mainly due to the effects of seasonal and episodic rainfall on hydrology and the Mississippi River diversion management that cause variability in the timing and magnitude of the nutrient-rich freshwater discharge to the estuary (Bargu et al., 2011; Roy et al., 2013; White et al., 2009). Nutrient and sediment input through BCS can result in significant changes in dissolved inorganic nitrogen concentrations (Lane et al., 2001; White et al., 2009) that can potentially trigger the enhanced primary production and cause phytoplankton community shifts. Additionally, there is a significant increase of P in the newly deposited river sediment, which can slowly be released over ensuing years further impacting estuarine water quality (Roy et al., 2012).

Chao et al. (2013, 2016) revealed that a large amount of sediment is discharged into Lake Pontchartrain, moving eastward and expanding northward after the opening of the BCS. Retana (2008) conducted a series of sensitivity experiments using the Finite Volume Community Ocean Model (FVCOM) for the hydrodynamic response during an opening of BCS. Chilmakuri (2005) suggested that a spatially variable- counter-clockwise wind in the middle of the lake is able to direct the plume from the BCS eastward.

Huang and Li (2017) and Li et al. (2018a) investigated the wind-driven circulation in the LPE under barotropic conditions. The remote wind controls the overall setup of the water level variation, while local wind determines the surface slope (Huang & Li, 2017). A quasi-steady state balance is verified in this system as well as in other coastal water bodies such as Barataria Bay (Li et al., 2019), and Elson Lagoon in the Arctic region (Li et al., 2019). This quasi-steady state balance is reached because the adjustment to wind variation in the form of a seiche in such a small system is fast enough to reach a new balance over a time scale shorter than a tidal cycle: The wind-driven seiche would be dissipated within two to three cycles lasting several hours (Li et al., 2018). A recent work by Huang and Li (2019) allowing density variation further confirms that the quasi-steady balance is asymmetric in the along- and cross-estuary directions: The R^2 value between the slope from the quasi-steady balance and that from the model result is lower in the east-west direction because of the impact of the eastern open boundary. However, the R^2 is still very high (>0.9).

Given all the work done, the study of the dynamics of the plume induced by artificial freshwater diversions in Lake Pontchartrain has rarely been done. Part of the reason is that the event has been rare until more recently. The impact however, as discussed in the papers mentioned above (Bargu et al., 2011; Chao et al., 2013, 2016; McCorquodale et al., 2009), is significant. Especially considering the fact that what used to be decadal events now have become much more common (almost annually, i.e., 2016, 2018, and 2019). The spillway was opened in 2018 and 2019, the first time ever in back to back years. It is therefore of much greater interest in learning the dynamical processes and the impact to the ecosystem, which is dependent on the former. Here we take advantage of a numerical model developed for this estuary and use the 2011 diversion event as a subject to conduct such a study with numerical experiments. The 2011 event had the largest total discharge in the five diversion events of the last decade, before this year (2019). We also have the advantage of clear satellite images for model consistency verifications.

More specifically, in this study, we use a 3-D FVCOM to simulate the freshwater diversion plume from the BCS of 2011 to 1) examine the impact of wind from cold fronts on the evolution of the freshwater plume from the BCS; 2) analyze the sensitivities of total salt contents, vertical structure of salinity, and currents to the magnitudes and directions of wind; 3) illustrate the effect of the minor leakage of river water from the BCS before opening of the diversion on the salinity, circulation pattern, stratification, and quasi-steady state balance; and 4) discuss the influence (residence) time of the freshwater inside the estuary and compare it with that from Lagrangian particle tracking.

2. Study Area and Data Description

The LPE (Figure 1) is a large ($\sim 1,600 \text{ km}^2$), shallow ($\sim 4 \text{ m}$), and almost enclosed estuary connected to the Gulf of Mexico through three narrow inlets: the Rigolets, Chef Menteur, and Industrial Canal. It has an oval shape with the longer axis ($\sim 66 \text{ km}$) in the east-west direction and the shorter axis ($\sim 40 \text{ km}$) in the north-south direction with a total volume of about $9.77 \times 10^9 \text{ m}^3$ (Keddy et al., 2007). The average salinity of the

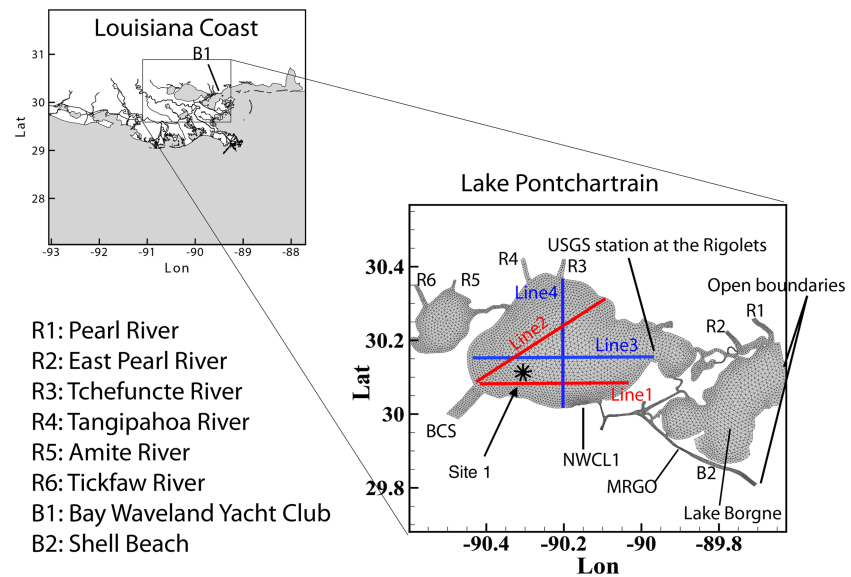


Figure 1. Study site and model mesh. BCS is the Bonnet Carré Spillway, NWCL1 is the NDBC station from where the wind and atmospheric data are obtained. Line1 and line 2 are used to show the vertical structures of velocity during the development of the freshwater plume. Line 3 and line 4 are selected to illustrate the vertical structure of the salinity and current distribution in the sensitivity experiments of wind magnitudes. Site 1 (star symbol) represents the site of the ADCP survey recording the velocity structure on 11 May 2011.

LPE is about 4. The bottom salinity can reach as high as 12 (Li et al., 2008). The city of New Orleans is located south of the LPE. Lake Pontchartrain has been used for river flood diversion to protect New Orleans through a control structure, the BCS. The spillway is located at the southwestern corner of the estuary connecting the LPE with Mississippi River. The spillway is about 9 km in length and the control structure consists of 350 “bays” each about 2.9 m wide. The structure allows a maximum of $\sim 7,000 \text{ m}^3 \cdot \text{s}^{-1}$ of Mississippi River water to be diverted into the estuary (Bargu et al., 2011). The BCS was opened after heavy rains in the Mississippi River and Ohio River valleys increased river stages on 9 May 2011 to prevent the Mississippi River flows at New Orleans from exceeding $35,000 \text{ m}^3/\text{s}$ (Allison et al., 2013). The spillway was completely closed again on 20 June 2011. The daily discharge from BCS can be obtained from the U.S. Army Corps of Engineers website (<https://www.mvn.usace.army.mil/>) and is shown in Figure 2. According to the U.S. Army Corps of Engineers, there is an amount of freshwater from Mississippi River that leaks into the LPE through the small spaces between the wooden timbers that hold back the water in each bay. This leakage is referred to as a minor diversion each year and occurs a few weeks in the spring or early summer when river stage exceeds the elevation of the spillway. The amount of the leakage is usually less than $300 \text{ m}^3/\text{s}$ (<https://www.mvn.usace.army.mil/>) but may increase due to prolonged river flood stage.

In this study, observations of water level used for model validation are from National Oceanic and Atmospheric Administration’s (NOAA) New Canal Station (ID: 8761927: $30^\circ 1.6' \text{N}$ and $90^\circ 6.8' \text{W}$). Salinity data used for model validation are from an U.S. Geological Survey (USGS) station at Hwy 90 near Slidell (USGS 2010011089442600, $30^\circ 10' 01'' \text{N}$, $89^\circ 44' 26'' \text{W}$, Figure 1) from 1 January 2011 to 30 September 2011. Velocity data recorded by an acoustic Doppler current profiler (ADCP) mounted on a small boat during a brief survey at the edge of the plume on 11 May were used to validate the two-layered flow inside of the LPE (Site 1 in Figure 1). The vessel-based survey used a small boat, a surface thermosalinograph, and a 1,200-KHz ADCP mounted in front of a 24-ft small boat. The thermosalinograph is the SBE 45 with a pump that fetches water from the surface so that the water temperature and salinity are measured and recorded at 10-s ensemble intervals. The measurements were done zigzagging across an apparent frontline in the middle of the Lake between 1856 UTC and 1949 UTC on 11 May 2011. The ADCP was used at almost the same time for the cross-frontal measurements. The ADCP was installed at $\sim 0.4 \text{ m}$ below the surface, and it was set up to measure the current velocity profile at 0.25-m vertical intervals every second. Data were averaged every 20 s.

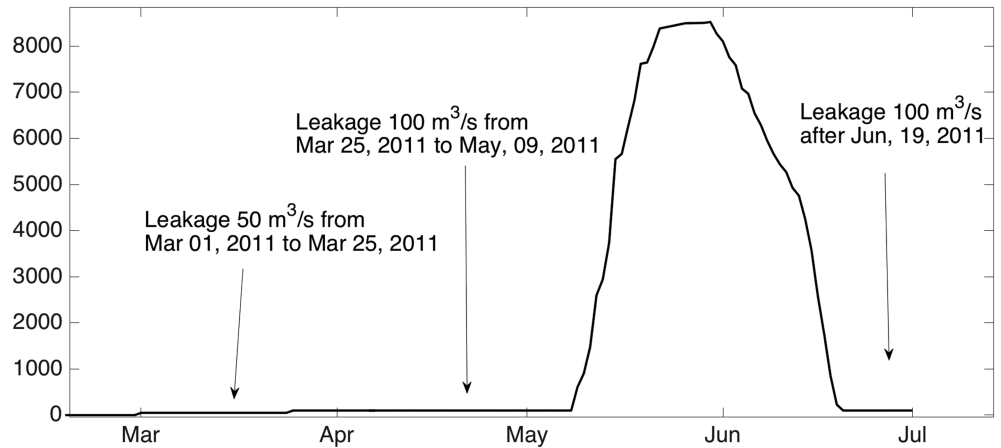


Figure 2. Freshwater discharge from BCS and the leakage added in the model.

The daily salinity and temperature data used for the open boundaries are from USGS stations at Mississippi Sound (ID: 300722089150100) and Black Bay (ID: 07374526) from 1 July 2010 to 30 September 2011. Wind and air pressure data at 6-min intervals are the National Data Buoy Center meteorological observation at the NWCL1 station. Daily river discharge data for the model input are from USGS stations of Pearl River (R1 in Figure 1, USGS 02490500), East Pearl River (R2 in Figure 1, USGS 02492110), Amite River (R5 in Figure 1, USGS 07380120), Tangipahoa River (R4 in Figure 1, USGS 07375500), Tchefuncte River (R3 in Figure 1, USGS 07375000), and Tickfaw River (R6 in Figure 1, USGS 07376000) between 1 July 2010 and 30 September 2011. Water elevation and tide prescribed at the open boundary are the hourly data from NOAA's stations: Bay Waveland Yacht Club, MS (B1 in Figure 1, Station ID: 8747437, 30°19.5'N, 89°19.5' W), for the eastern open boundary and Shell Beach, LA (B2 in Figure 1, Station ID: 8761306, 29°52.1'N, 89°40.4'W), for the southeastern open boundary. The observational data from these two NOAA stations are used to represent the water level variation of all nodes in each of the two open boundaries.

3. Model Description

FVCOM has been widely used for studying coastal ocean hydrodynamics, especially for regions with complicated topography (Chen et al., 2003). The governing equations are (Chen et al., 2003):

$$\frac{\partial u}{\partial t} + u \frac{\partial u}{\partial x} + v \frac{\partial u}{\partial y} + w \frac{\partial u}{\partial z} - fv = -\frac{1}{\rho_0} \frac{\partial P}{\partial x} + \frac{\partial}{\partial z} \left(K_m \frac{\partial u}{\partial z} \right) + F_u, \quad (1)$$

$$\frac{\partial v}{\partial t} + u \frac{\partial v}{\partial x} + v \frac{\partial v}{\partial y} + w \frac{\partial v}{\partial z} + fu = -\frac{1}{\rho_0} \frac{\partial P}{\partial y} + \frac{\partial}{\partial z} \left(K_m \frac{\partial v}{\partial z} \right) + F_v, \quad (2)$$

$$\frac{\partial w}{\partial t} + u \frac{\partial w}{\partial x} + v \frac{\partial w}{\partial y} + w \frac{\partial w}{\partial z} = -\frac{1}{\rho_0} \frac{\partial p}{\partial z} + \frac{\partial}{\partial z} \left(K_m \frac{\partial w}{\partial z} \right) + F_w - g, \quad (3)$$

$$\frac{\partial u}{\partial x} + \frac{\partial v}{\partial y} + \frac{\partial w}{\partial z} = 0, \quad (4)$$

$$\frac{\partial T}{\partial t} + u \frac{\partial T}{\partial x} + v \frac{\partial T}{\partial y} + w \frac{\partial T}{\partial z} = \frac{\partial}{\partial z} \left(K_h \frac{\partial T}{\partial z} \right) + F_T, \quad (5)$$

$$\frac{\partial S}{\partial t} + u \frac{\partial S}{\partial x} + v \frac{\partial S}{\partial y} + w \frac{\partial S}{\partial z} = \frac{\partial}{\partial z} \left(K_h \frac{\partial S}{\partial z} \right) + F_S, \quad (6)$$

$$\rho = \rho(T, S, p), \quad (7)$$

where x , y , and z are the three axes in the east, north, and vertical directions, respectively; u , v , w , T , and S are the x , y , and z velocities, temperature, and salinity, respectively; ρ_0 is the reference density specified as 1,000

kg/m^3 ; ρ is the density which is a function of temperature, salinity, and pressure; P is the total pressure of air and water; f is the Coriolis parameter; g is the gravitational acceleration; K_m is the vertical eddy diffusion coefficient, determined by the Mellor and Yamada (1982) level-2.5 (MY-2.5) turbulent closure scheme modified by Galperin et al. (1988); K_h is the thermal vertical eddy diffusion coefficient; and F_u , F_v , F_T , and F_S are the diffusion terms for the horizontal momentums, thermal, and salt in x and y directions, respectively.

The surface and bottom boundary conditions are

$$K_m \left(\frac{\partial u}{\partial z}, \frac{\partial v}{\partial z} \right) = \frac{1}{\rho_0} (\tau_{sx}, \tau_{sy}), w = \frac{\partial \zeta}{\partial t} + u \frac{\partial \zeta}{\partial x} + v \frac{\partial \zeta}{\partial y}, \text{ at } z = \zeta(x, y, t), \quad (8)$$

$$K_m \left(\frac{\partial u}{\partial z}, \frac{\partial v}{\partial z} \right) = \frac{1}{\rho_0} (\tau_{bx}, \tau_{by}), w = -u \frac{\partial H}{\partial x} - v \frac{\partial H}{\partial y}, \text{ at } z = H(x, y), \quad (9)$$

where (τ_{sx}, τ_{sy}) and (τ_{bx}, τ_{by}) are surface wind stress and bottom stress vectors, respectively. H is the water depth and ζ is the free surface elevation. (τ_{sx}, τ_{sy}) is calculated by $C_d \rho_a |U_{10}| U_{10}$, where U_{10} is the wind at 10-m height, ρ_a is the air density (1.29 kg/m^3), and C_d is the surface wind drag coefficient and is calculated by the scheme of Large and Pond (1981) as showing in the following equations:

$$C_d = \begin{cases} (0.49 + 0.065 \times 11.0) \times 10^{-3}, & U_{10} < 11.0 \text{ m/s}, \\ (0.49 + 0.065 \times |U_{10}|) \times 10^{-3}, & 11.0 \frac{\text{m}}{\text{s}} \leq U_{10} \leq 25.0 \text{ m/s}, \\ (0.49 + 0.065 \times 25.0) \times 10^{-3}, & U_{10} > 25.0 \text{ m/s}. \end{cases} \quad (10)$$

(τ_{bx}, τ_{by}) is calculated by $C_d \sqrt{u^2 + v^2} (u, v)$, where C_d here is the drag coefficient and is determined by the following:

$$C_d = \max \left(\frac{k^2}{\ln \left(\frac{z_{ab}}{z_0} \right)^2}, 0.0025 \right), \quad (11)$$

where k is the von Karman constant (0.4), z_0 is the bottom roughness parameter, and z_{ab} is the height above the bottom.

The model mesh has 6,053 nodes and 10,580 cells (Figure 1). The two open boundaries are located at the east of Lake Borgne and the south end of Mississippi River Gulf Outlet, respectively. In this study, we only simulate the hydrodynamics during the opening in 2011. The simulation time period is from 2010/07/01 to 2011/09/30. The water level at the two open boundaries is provided by hourly observations from the two NOAA's stations mentioned earlier. Spatially uniform and temporally changing wind and air pressure are included for the atmospheric forcing. River discharges from seven rivers (Pearl River, East Pearl River, Amite River, Tangipahoa River, Tchefuncte River, and Tickfaw River) are included. During the opening of the BCS, discharge at the diversion structure is included as a river from the spillway from 9 May 2011 to 19 June 2011. All salinities for these rivers are set to be 0. Temperatures for these rivers are given as the same as the observed temperature of a USGS station at Rigolets at Hwy 90 near Slidell. The initial salinity and temperature are obtained from the USGS observation at Rigolets at Hwy 90 near Slidell on 1 July 2010, which are set to be constant 1.7 and 28.7 °C for all nodes. In simulating the freshwater diversion, it is reasonable to add an amount of freshwater discharge due to the minor leakage during flood season. Since there is no measurement of leakage, we can only test our model adding a small amount of leakage by trial and error. Results show that when the leakage is set to be 50 m^3/s from 1 to 25 March 2011, 100 m^3/s from 25 Mar 2011 to 9 May 2011, and 100 m^3/s from June 2011 to the end of simulation (Figure 2), the skill score of the simulation of salinity is increased from 0.64 (blue line in Figure 3b) to 0.78 (black line in Figure 3b), indicating that the leakage added in our numerical experiments is reasonable.

To examine the wind effect and the influence of the opening of the BCS, six groups of experiments are conducted (Table 1). For all of the following experiments, salinity and temperature are provided at the open boundary. Experiment 1 reproduces the real case using observed water level at the open boundaries and

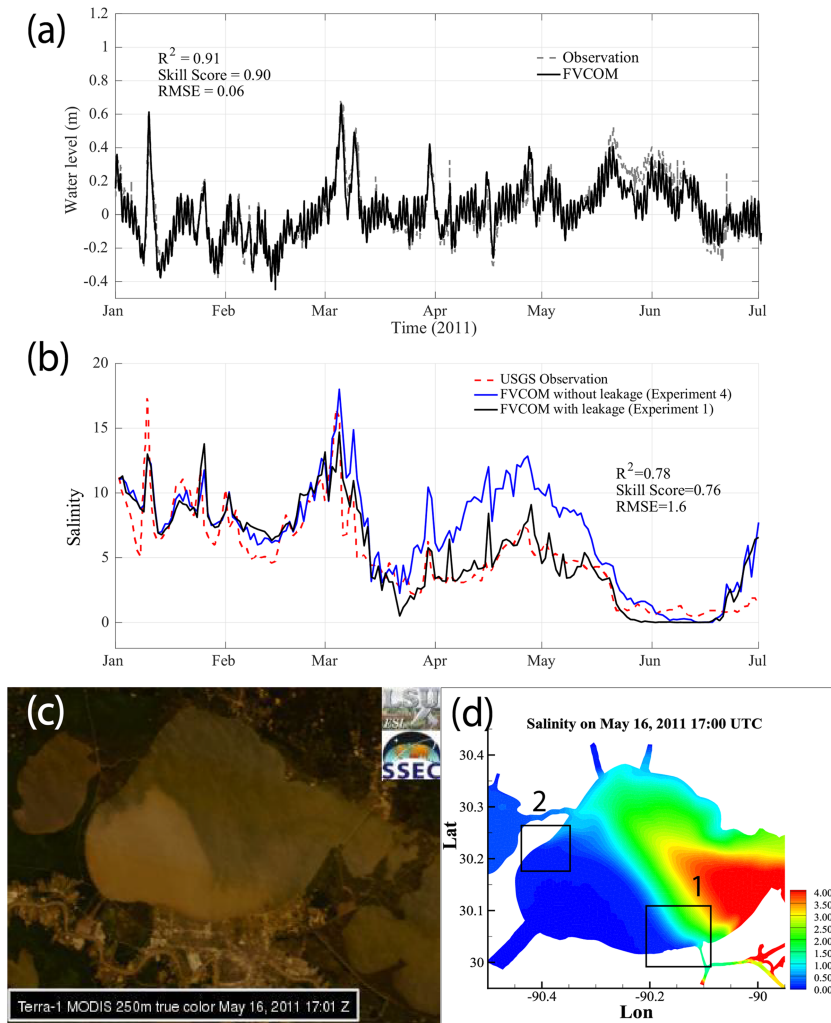


Figure 3. Validation of water level at New Canal (a) and salinity at the USGS station near the Rigolets (b). Solid black lines represent the model results (Experiment 1) with the leakage effect; solid blue line is the salinity simulated by Experiment 4, excluding leakage effect; dashed gray lines represent the observations; R^2 , skill score, and RMSE are evaluated for the Experiment 4; (c) is the satellite image from ESL of LSU; light brown color represents river waters and dark brown represents areas outside of the river plume; and (d) is from the model result. Rectangular 1 indicates the angle between the front edge of the plume and the coastline in the southern shore. Rectangular 2 shows that in the western shore.

Table 1
Model design for two groups of numerical modeling.

Period	07/01/2010–05/09/2011		05/09/2011–06/19/2011 (opening of BCS)		06/19/2011–09/30/2011		Description
	Forcing	BCS	Forcing	BCS	Forcing	BCS	
1	Wind + observed water level	close	Wind + observed water level	Open	Wind + observed water level	Close	Real case with leakage
2	No wind + tide	close	No wind + tide	Open	No wind + tide	Close	Tidal effect with leakage
3	Wind + observed water level	close	Wind + observed water level	Close	Wind + observed water level	Close	Impact of river diversion
4	Wind + observed water level	close	Wind + observed water level	Open	Wind + observed water level	Close	Real case without leakage
5	—	—	Wind Increases from 2 to 14 m/s	Open	—	—	Sensitivity experiments
6	No wind + tide	close	No wind + tide	Open	No wind + tide	Close	Tidal effect without leakage

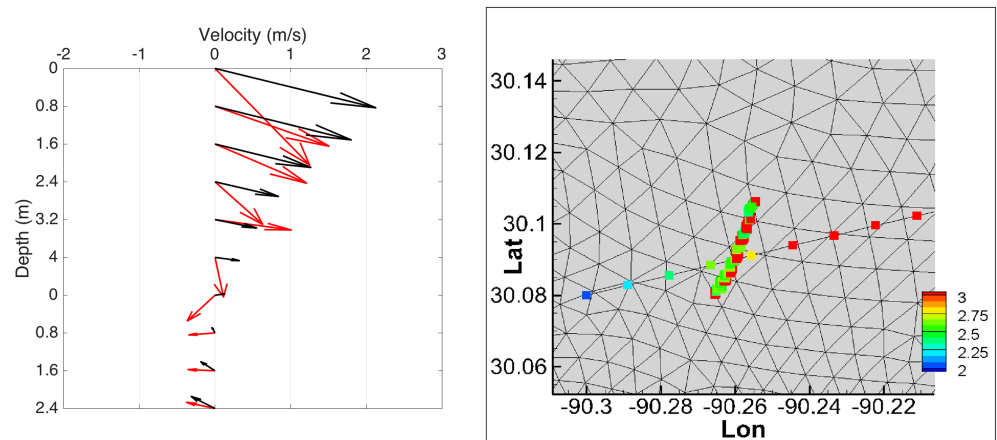


Figure 4. Comparison between the vertical structure of velocity from the FVCOM model (black vectors) and that from the survey (red vectors) on 11 May 2011. The left panel is the instantaneous velocity comparison between the model and observations, while the right panel is the instantaneous comparison for salinity: The colored dots in the right panel are salinity from model output in PSU along the model grids (along roughly the east-west direction) and the observations in PSU along the ship track (along roughly the north-south direction).

the observed wind forcing for all nodes of the study area. Since the observed water level prescribed at the open boundary contains a complex response to nonlocal weather forcing (Huang & Li, 2019), Experiment 1 simulates the combined effect including local and remote wind effect, which is the closest to the real condition. Experiment 2 excludes wind effect by only applying tidal forcing at the open boundaries. Leakage is included in both Experiments 1 and 2. The comparison between Experiments 1 and 2 reveals the influence of wind. Experiment 3 excludes the influence of the freshwater diversion by closing the BCS. This experiment aims at investigating the influence of freshwater diversion during the opening of the BCS. Experiment 4 simulates the condition without the leakage at the diversion but with wind stress applied on the surface and observed water level forced at the open boundary. It is exactly the same as Experiment 1 except that no leakage is included. Experiment 5 is a series of simulations during the opening of the spillway from 9 May to 19 June 2011. There are 28 cases in the Experiment 5. Observed water level is applied at the open boundary for all of these experiments. Northerly, southerly, easterly, and westerly wind are added as the atmospheric forcing. Wind magnitude increases from 2 to 14 m/s under each wind direction. Leakage effect is excluded. These experiments are used to examine the sensitivity of circulations and salinity to wind direction and wind magnitude. Experiment 6 is similar with Experiment 4, but no wind is added, which only contains tidal effect when leakage is excluded.

As shown in Figure 3a, the performance of FVCOM in simulating the water level can be categorized as excellent with a skill score of 0.9 according to Allen et al. (2007). The simulated salinity near the Rigolets exhibits an excellent performance (skill score is 0.78) when compared with the observations (Figure 3b). Satellite image (Figure 3c) shows the true color of the Lake Pontchartrain on 16 May 2011. Since freshwater diversion from Mississippi river can transport large amount of sediment into the Lake Pontchartrain, so the light brown color of the true color satellite image can reflect the shape of the freshwater plume from the BCS. Surface salinity contour plots are consistent with the satellite images (Figure 3d).

The model results show clear and persistent two-layered flows. The analytic model and FVCOM in Li et al. (2008) demonstrated the wind-driven two-layered flow. In Li et al. (2018a), the two-layered flows were also demonstrated that are consistent with theories presented in Englund (Englund, 1973). Here we further compare the model results with the in situ observations. Comparison between the vertical structure of velocity from FVCOM model (black arrows) and that from the survey (red arrows) on 11 May 2011 is shown in Figure 4a. Clearly, the observations also show a two-layered flow structure, and the FVCOM model is able to reproduce it. The model also produced the correct vertical position of the no-flow level. The front location of the plume and the salinity of the two sides of the front are correctly reproduced compared with the observations on 11 May 2011 (Figure 4b).

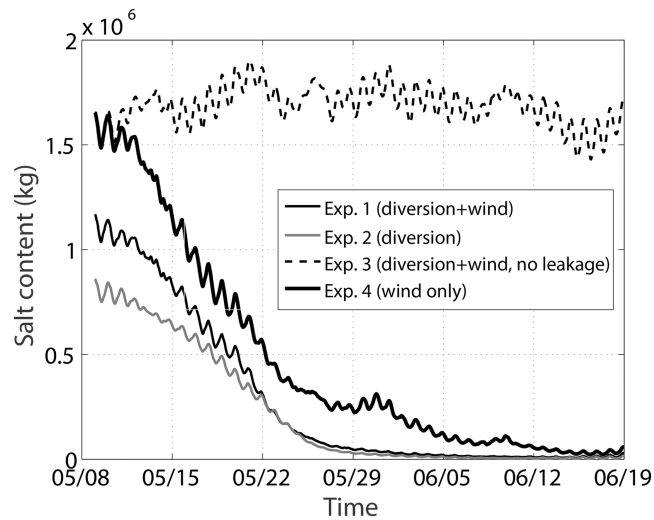


Figure 5. Salt content from Experiment 1 (thin black line), Experiment 2 (gray line), Experiment 3 (dashed line), and Experiment 4 (thick line).

4. Results

4.1. Evolution of Freshwater Plume

With the opening of BCS from 9 May 2011, freshwater was diverted into Lake Pontchartrain. Salt content is calculated using the following equation:

$$Mass_{salt}(t) = \sum_{i=1}^{ncell} \int_{-h}^{\zeta} S(i, z, t) \times A(i) dz, \quad (12)$$

where $Mass_{salt}(t)$ is the total mass of salt for the whole study area at time t ; $ncell$ is the total number of cells of the mesh and equals 10,580 in our model; h and ζ represent water depth and free surface elevation, respectively; $S(i, z, t)$ is salinity for the i th cell at a given water depth z at time t ; $A(i)$ is the area for the i th cell; and z is the vertical position. Figure 5 shows the time series of salt content from Experiments 1 (real case simulation), 2 (only diversion and tide are included, no wind forcing), and 3 (there is no diversion). Solid black line (Experiment 1) in Figure 5 shows the time series of salt content variation during the opening of the spillway. It is found that salt content was decreasing during the first 10 days of the opening, and maintained a relatively low value after May. The shape of the freshwater plume on 16 May can be shown by satellite image and model results in Figures 3c and 3d, the plume with more suspended sediment from the Mississippi river was diverted into Lake Pontchartrain. The edge of the front of the plume was asymmetric, the southeastern edge of the plume, and the southern shoreline formed an acute angle pointing to the east (rectangle 1 in Figure 3d), while the western edge and the western shoreline formed an obtuse angle that is pointing to the south (rectangle 2 in Figure 3d). As the freshwater being continuously diverted into the lake, the area of the plume expanded into the whole lake after 5 June 2011.

According to Li et al. (2018a), wind determines the flow pattern inside the lake, current flows in the direction with wind along the nearshore area and against the direction of the wind in the central interior of the lake (Huang & Li, 2017; Li et al., 2018a). Huang and Li (2017, 2019) also prove that flows of the Lake Pontchartrain reach a quasi-steady state balance under changing wind on both barotropic and baroclinic condition through two to three cycles of seiches within several hours (Li et al., 2018a). Therefore, the instant flow snapshot can be used to investigate how different wind directions can affect the circulations of Lake Pontchartrain. The following examines how wind controls the current and the plume in Lake Pontchartrain. Figure 6 shows how the shape of the plume is affected by wind. The plumes with or without wind are compared. Figures 6a, 6c, 6e, and 6g are real case simulations (Experiment 1) under southerly (12:00 UTC, 13

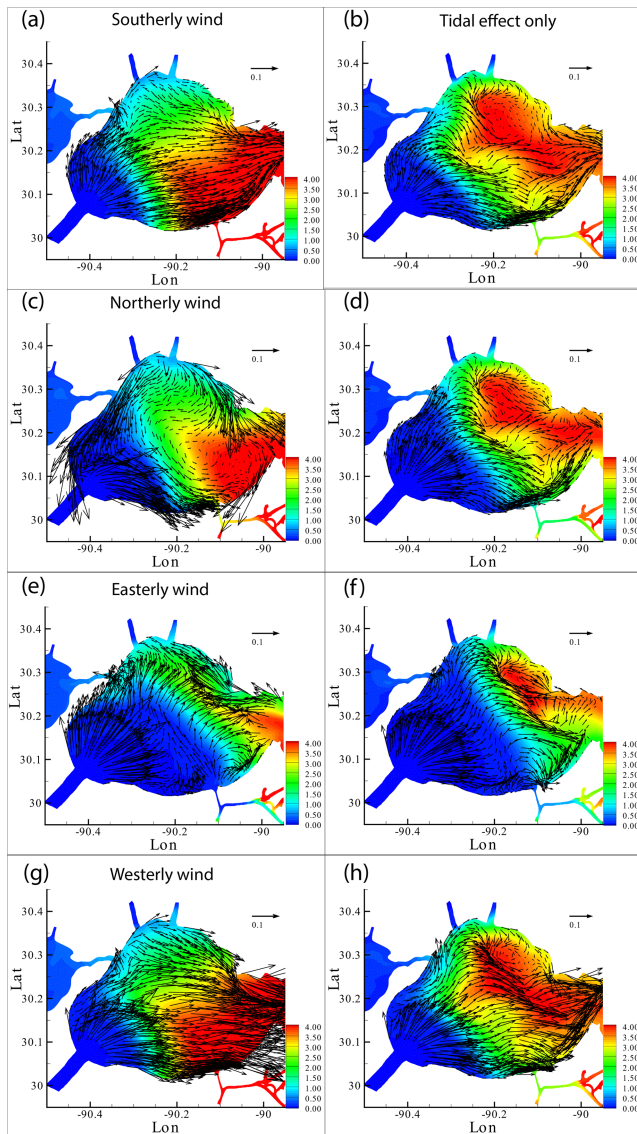


Figure 6. Salinity and velocity vector during four different wind directions from experiments 1 and 2. Figures 6a, 6c, 6e, and 6g are real case simulation (Experiment 1) under southerly (12:00 UTC, 13 May), northerly (12:00 UTC, 15 May), easterly (16:00 UTC, 18 May), and westerly (00:00 UTC, 18 May) winds. Figures 6b, 6d, 6f, and 6h are the cases simulated only under tidal effect and the wind effect was excluded (Experiment 2). Leakage was included. Arrows are current vectors.

May), northerly (12:00 UTC, 15 May), easterly (16:00 UTC, 18 May), and westerly (00:00 UTC, 18 May) winds, respectively. Figures 6b, 6d, 6f, and 6h are results with only tidal forcing (Experiment 2). During southerly wind (Figures 6a and 6b), the western edge of the plume resulted from Experiment 1 is extended further to the northern area compared with that of Experiment 2, while the southeastern edge of the plume from Experiment 1 is constrained further to the west compared with that from Experiment 2. Northerly wind tends to limit the expansion of the freshwater plume. The comparison between Figures 6c and 6d shows that during northerly wind, the area of the plume from Experiment 1 (the region with salinity lower than 0.2 in Figure 6c) is apparently smaller than that from Experiment 2 (Figure 6d), which is simulated without wind.

Easterly wind facilitates the inward flow from the eastern open boundary, compressing the plume and keeping it from expanding to the northern and eastern region (Experiment 1) (Figure 6e), so that the edge of the plume is more restricted to the western area than that from Experiment 2 (Figure 6f). Westerly wind pushes the plume from Experiment 1 (Figure 6g) to eastern area than that from Experiment 2 (Figure 6h), making the shape of the plume from Experiment 1 more elongated in the east-west direction than that from Experiment 2.

Above all, the southwestern edge of the freshwater plume can be extended to the east by the westerly along shore flows induced by the westerly wind, while easterly and northerly winds tend to compress the plume from extending to the northern area, and southerly wind facilitates the plume's expansion to the northern area. In addition, northerly and southerly wind tend to make the shape of the plume more asymmetric compared with that under tidal effect.

4.2. Impact of Wind Associated With Cold Fronts

Winds during atmospheric frontal passages have significant impact on the hydrodynamics in coastal waters. For example, hydrodynamic responses to 76 atmospheric front events in a tidal channel in the southern Louisiana are found to be highly correlated with the atmospheric forcing: cold (warm) fronts can produce outward (inward) transports (Li et al., 2018; Weeks et al., 2018). In addition, southerly winds prior to a cold front event can drive saltwater intrusion (Li et al., 2011; Lin et al., 2016). There were three atmospheric fronts affecting the study area during the opening of the BCS (vertical lines in upper panel of Figure 7) on 06:00 UTC, 14 May; 06:00 UTC, 18 May; and 18:00 UTC, 27 May, respectively. The first cold front is denoted by the change of wind direction from south to northwest (Figure 7). Wind for the second cold front changes its direction from north to southeast. The third cold front is represented by the transient wind direction from northeast to southwest. The common feature of the three cold fronts is that there is a relatively long period (more than 18 hr) when southerly wind dominated. Wind magnitudes for the time of the three snapshots being selected are 4, 3, and 6 m/s, respectively.

To illustrate the vertical structure of salinity and current, nodes along two lines are selected (Figure 1). Line 1 is along the southern coast in east-west direction, line 2 has a 45° inclination from the east-west direction and is along the orientation of the BCS. Velocities are all rotated to be along and cross the lines. Only the along-line components are plotted in Figure 7. On 14 May, the currents along both lines 1 and 2 exhibit two-layered structures (Figure 7a and 7d). Wind on 14 May is overwhelmingly from the southern quadrants (wind vector in Figure 7). The water columns along both lines 1 and 2 are almost well mixed but with vertical shears of horizontal velocity as demonstrated by the top layer water flowing away from BCS and bottom water flowing back toward BCS at lower layer (Figures 7a and 7d). The circulation patterns are consistent

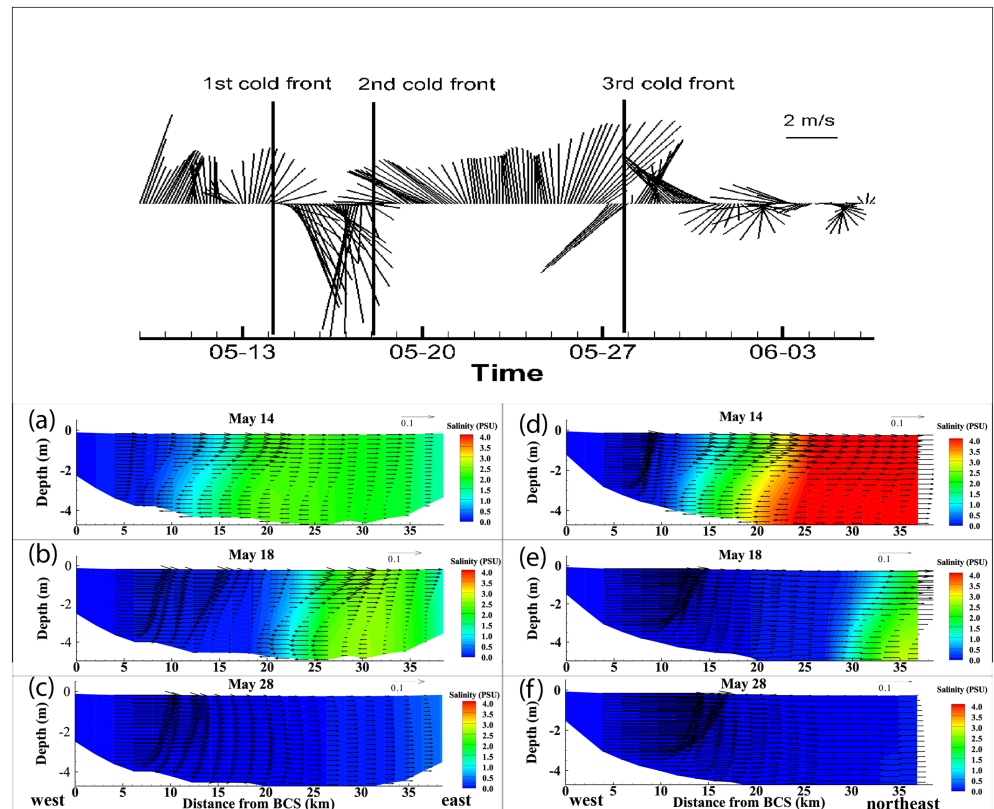


Figure 7. Upper panel is the wind vector from 9 May to 6 June. Vertical black lines represent the dates of three cold front event during this time period. Lower panel is the vertical structure of salinity and along-line velocity for nodes along line 1 (a–c) and line 2 (d–f) on different dates. Results are from Experiment 1. Dates represent the time for three cold front passages during the freshwater diversion period. Arrows are along-line current.

with the work by Li et al. (2018a) and Huang and Li (2019), that is, surface current and the coastal current flow downwind, while bottom current in the lake flows against the wind. This is the case for 18 May (Figure 7e) and 28 May (Figures 7c and 7f) when southeasterly and southwesterly winds were dominating, except for Figure 7b that the water column is well mixed. The two-layered flows for the second cold front on 18 May are not as that obvious as that for the other two cold front events. The wind magnitude is only 3 m/s. The two-layer flow is the strongest during the cold front event on 28 May with wind magnitude reaching 6 m/s. The upper downwind layer is thickest for this cold front event. These results indicate that the thickness of the two-layered flow is related to wind magnitude: Higher wind magnitude can increase the thickness of the upper downwind flow. The following will further discuss how salinity and current are affected by increasing wind magnitude.

4.3. Effects of Magnitude of Wind

4.3.1. Sensitivity of Vertical Structure of Salinity and Currents

Two lines are selected to illustrate the vertical structure of the salinity distribution and the current in east-west (line 3 in Figure 1) and north-south (line 4 in Figure 1) directions, respectively. During easterly and westerly winds, when the wind magnitude changes from 4 to 12 m/s (Figure 8), the surface flow along line 3 is downwind, while the bottom flow upwind. Both surface and bottom flows become stronger when the wind magnitude increases. There is a no-motion plane between the two-layer flows (white lines in Figure 8). As the magnitude of the wind increases, the no-motion plane migrates downward to a lower layer. In terms of the salinity distribution under easterly wind, high salinity zone is located near the eastern side of the line. As easterly wind increases in magnitude, more saltwater is transported into the lake through the eastern open boundary. As a result, higher salinity zone expands to a larger area inside the lake. However, when wind is

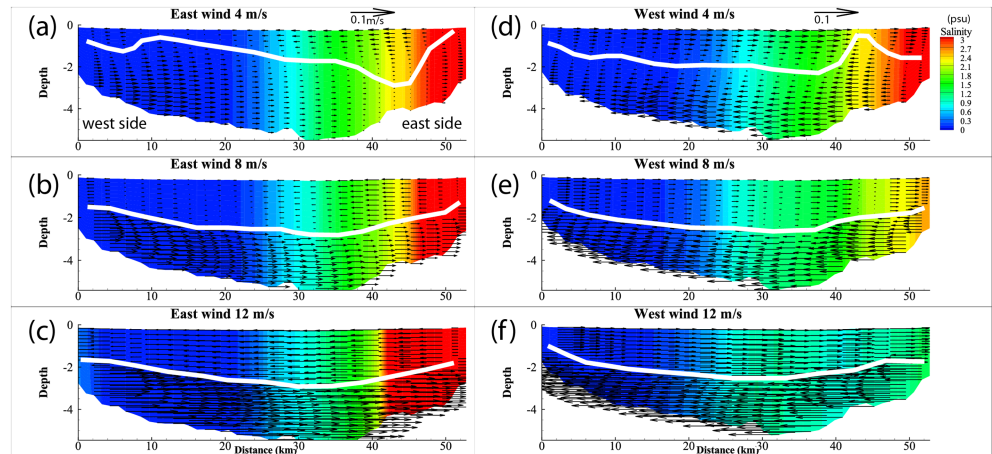


Figure 8. Vertical structure of along-line 3 velocity and salinity under easterly (a–c) and westerly winds (d–f). Unit of salinity is in psu. Results are from Experiment 5. Arrows are along-line current vectors.

blowing from the west, saltwater tends to be transported out of the lake through the eastern open boundary, leading to a smaller saltwater zone as the wind magnitude increases.

During northerly and southerly winds, when the magnitude of wind changes from 4 to 12 m/s (Figure 9), the surface flow along line 4 is downwind, and the bottom flow is upwind. Similarly, under easterly and westerly wind conditions, the surface and bottom flows become stronger when wind magnitude increases. Again, there is a no-motion plane between the two-layer flows (white lines in Figure 9), migrating to a deeper layer as the magnitude of wind increases. Since line 4 is north-south oriented with its southern side near the Industrial Canal, salinity along this line is affected more by the saltwater transported through the Industrial Canal at the southern end of the line. During northerly wind, the surface fresher water is transported to the southern end, leading to a fresher water zone located in the southern side. During southerly wind, saltwater is transported through Industrial Canal, resulting a high salinity zone at the southern end of line 4.

4.3.2. Sensitivity of Salt Content

Responses of salt content to increasing wind magnitude under the four wind directions (Experiment 5) is shown in Figure 10. The salt content is increasing as the magnitude of wind increases except for westerly wind. Under westerly wind, when wind magnitude is lower than 6 m/s, salt content is decreasing, when wind is larger than 6 m/s, salt content is increasing. This is because westerly wind tends to blow more freshwater from the spillway to the lake when wind is less than 6 m/s, when wind increases to larger than 6 m/s,

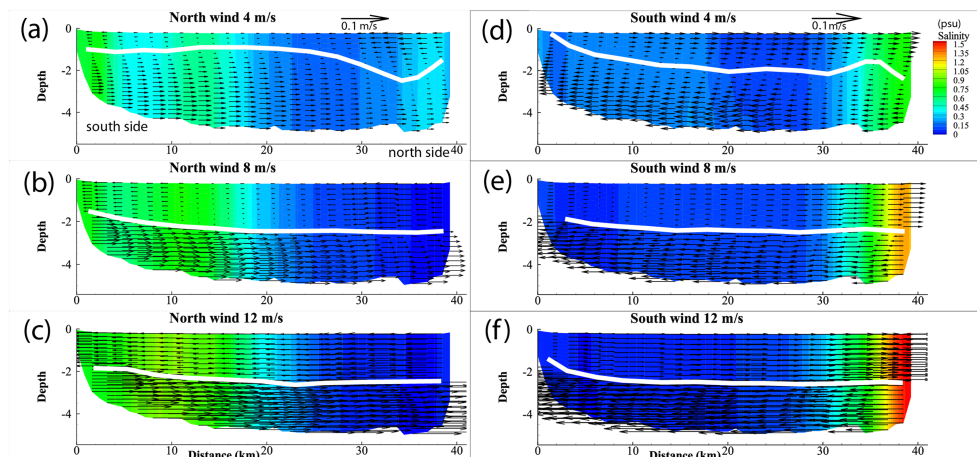


Figure 9. Vertical structure of along-line 4 velocity and salinity under northerly (a–c) and southerly winds (d–f). Unit of salinity is in psu. Results are from Experiment 5. Arrows are along-line current vectors.

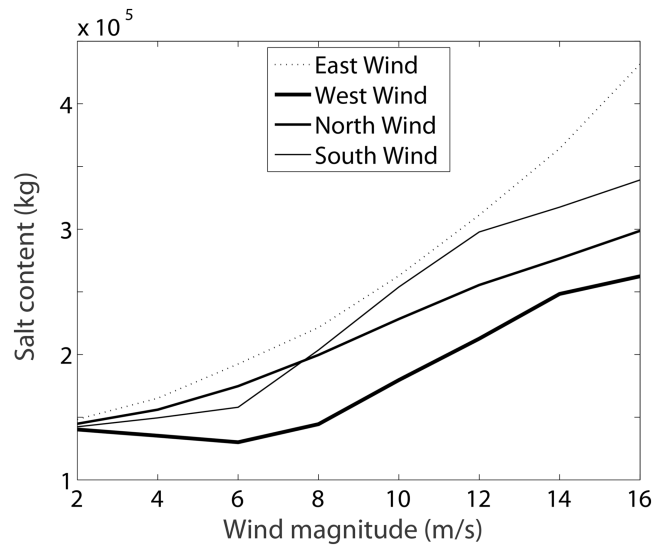


Figure 10. Sensitivity of salt content to increasing wind magnitude. Results are from Experiment 5.

saltwater from eastern open boundary is transported into the lake with a rate higher than that of the freshwater input from the BCS.

4.4. Leakage Effect on the Hydrodynamics of the Lake

4.4.1. Leakage Effect on Salt Content

An amount of freshwater leaks into Lake Pontchartrain through the BCS is added into the simulation. This amount of freshwater, though small compared with the diversion during the opening of the BCS, has great impact on the salinity distribution and salt content of Lake Pontchartrain. Blue line in Figure 3b shows the variation of salinity when leakage effect is excluded (Experiment 4). In general, the salinity is lower when the leakage is added. To illustrate the effect of the leakage on the salt content, we compare the results with (Experiment 1) or without the leakage (Experiment 4, Figure 5). After adding the freshwater leakage, salt content in the lake is only 800,000 kg at the beginning of the opening of spillway. The difference between the two experiments reaches 1,600,000 kg, which means that the leaked freshwater decreases the salt content in the lake by 2 times. During the overall opening period of the BCS, the salt content reduced by the leaked freshwater is about 3.7×10^8 kg.

4.4.2. Leakage Effect on Circulation Pattern

The influence of freshwater leakage from the Mississippi River can be illustrated by removing the leakage at the BCS (Experiments 6 and 7). Circulation and the salinity distribution without the leakage effect for the whole lake are shown in Figure 11. The frontal zone of the river plume is much closer to the BCS than that with the leakage (Figure 6). Salinity for the water near the eastern open boundary without leakage (Figure 11) is about 4–5 times higher than that in Figure 6. For the circulation, flows along the southern shore (Figure 11) is weaker than that with the leakage (Figure 6), indicating that the leakage can enhance the flow along the southern shore. Under northerly and southerly winds, the surface flows in the central lake are mainly against the wind (Figures 11a and 11c); however, this kind of return flow is not shown in Figure 6 when there is leakage. In addition, under easterly or westerly wind (Figures 11e and 11g), there are some minor but visible gyres in the northern central lake, which are not seen in Figure 6.

4.4.3. Leakage Effect on APED

The average potential energy demand (APED) for the whole lake is calculated using the following equation (Li et al., 2009; Simpson et al., 1990) to determine the water column gravitational stability:

$$\Phi = \frac{1}{h} \int_{-h}^{\zeta} (\bar{\rho} - \rho) g z \, dz, \quad (13)$$

where h and ζ represent water depth and free surface elevation, $\bar{\rho}$ and ρ represent the averaged density and in situ density, g is the gravity acceleration, and z is the vertical position. The larger the APED is, the more energy it needs to reach the vertically well-mixed conditions, or the more stratified the water column is.

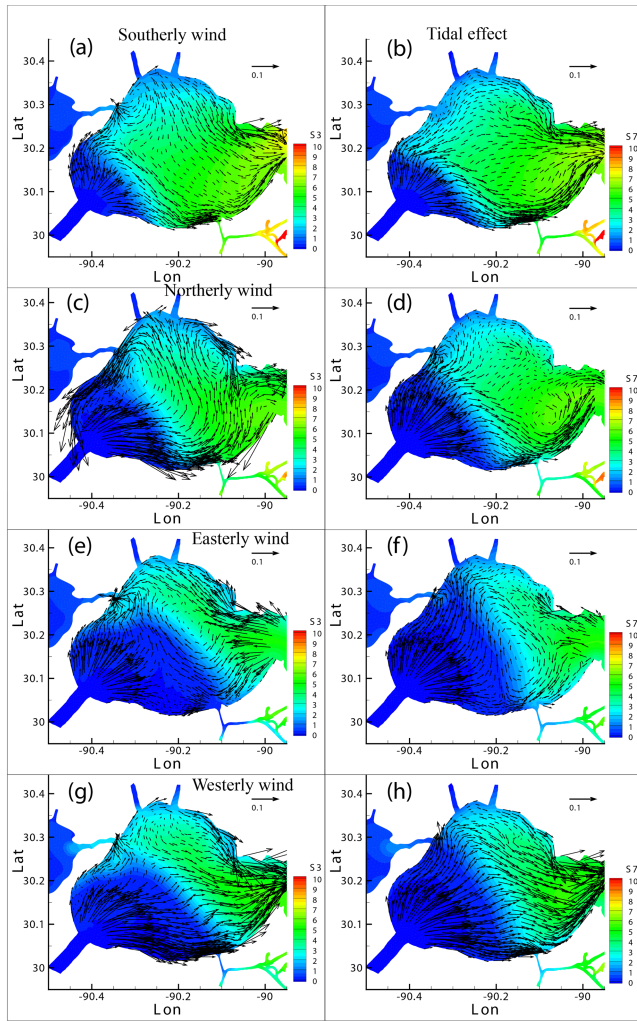


Figure 11. Salinity and velocity vector during four different wind directions from Experiments 4 and 6. Panels a, c, e, and g are without leakage effect from Experiment 4 under southerly, northerly, easterly, and westerly winds. Panels b, d, f, and h are the cases simulated only under tidal effect and the wind and leakage effect were excluded (Experiment 6). Arrows are current vectors.

saltier at 23 km away from the BCS (Figure 7a). In terms of the vertical structure of the horizontal velocity along the transect, the return flow in the lower layer on both lines 1 and 2 is stronger when leakage is excluded. This indicates that with the leakage, water in the Lake Pontchartrain tends to be well mixed and fresher. The leakage makes the salinity to drop dramatically, leading to an almost-zero density gradient in the horizontal.

4.4.5. Diversion and Leakage Effect on Quasi-Steady State Balance

Previous studies have shown that local wind is the main driver of the lake surface slope in the along- and cross-estuary directions and can be well approximated by a quasi-steady state force balance (Huang & Li, 2017; Li et al., 2018a, b; and Li et al., 2019a,b) in which no stratification was considered. This quasi-steady state balance is

$$0 = -g \frac{\partial \zeta}{\partial x} + \frac{\tau_{ax}}{\rho h}, \quad (14)$$

The results show that APED decreases no matter what the wind direction is, namely, the water column is more mixed as wind magnitude increases.

APED without leakage effect for a water column of each node is shown in Figure 12. It is found that high APED region from Experiment 4 (Figures 12a, 12c, and 12e) appears in a band, which is consistent with location of the edge of the freshwater plume from BCS. As the plume moved to the northeast, the peak values of APED decreases. When wind is excluded (Experiment 6, Figures 12b, 12d, and 12f), the band with high APED disappears. High APED area only shows in the eastern side, which may be resulted from saltwater intrusion from the open boundary. This indicates that wind has a straining effect (as discussed in Li et al., 2008) on the stratification of salinity along the edges of the freshwater plume when no leakage is added. When leakage of freshwater is added (Experiments 1 and 2), APED values are all decreased (Figures 13a, 13c, and 13e), meaning that water is more mixed than that without the leakage effect. One thing to be noted is that when wind is excluded on 19 May (Figure 13d), there is a larger APED value band under tidal effect compared with that under wind forcing, indicating that wind facilitates more mixing of the water in this area.

4.4.4. Leakage Effect on Salinity and Velocity

To illustrate the leakage effect on the vertical structure of the circulation and salinity distribution, Figure 7 is compared with Figure 14. From Figure 14, one can see that on 14 May, the velocity along both lines 1 and 2 exhibits two-layered structures. A weak vertical variation in the water column of line 1 is seen at about 16 km away from the BCS, where the surface velocity reaches its maximum with freshwater on top of the slightly saltier water in the bottom layers. On line 2, water at 10 to 24 km away from the BCS shows slight vertical change in salinity. A strong return flow in the bottom layer can be seen. The vertical structures of salinity on 18 and 28 May are similar to that on 14 May. A sign of slight stratification can be seen at the front between the river water from the BCS and the surrounding water. Generally, the plume from the BCS in the southwestern corner spread to the northeastern part of the lake.

Compared with the salinity distribution shown in Figure 7, salinity in Figure 14 is higher by 4 PSU, the horizontal salinity difference (4) is also much larger than that shown in Figure 7 (0.5). The saltier water zone is more extended into the interior, for example, on 16 May, the water becomes saltier at 10 km away from the BCS (Figure 14a). However, it is

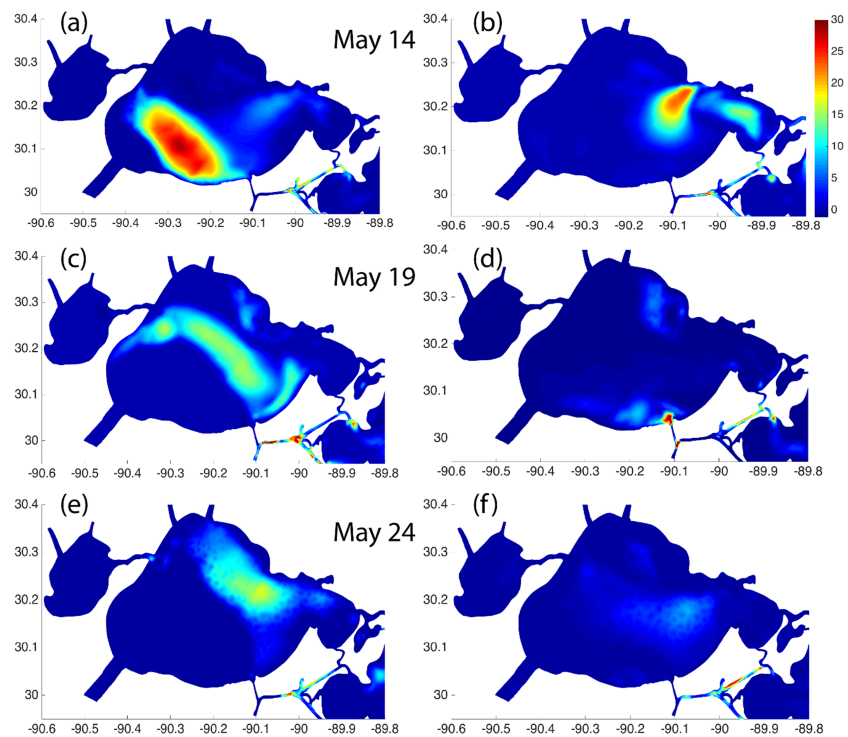


Figure 12. Average potential energy demand (APED) contour plot during three cold front events. Panels a, c, and e are results from Experiment 4; panels b, d, and f are calculated using Experiment 6.

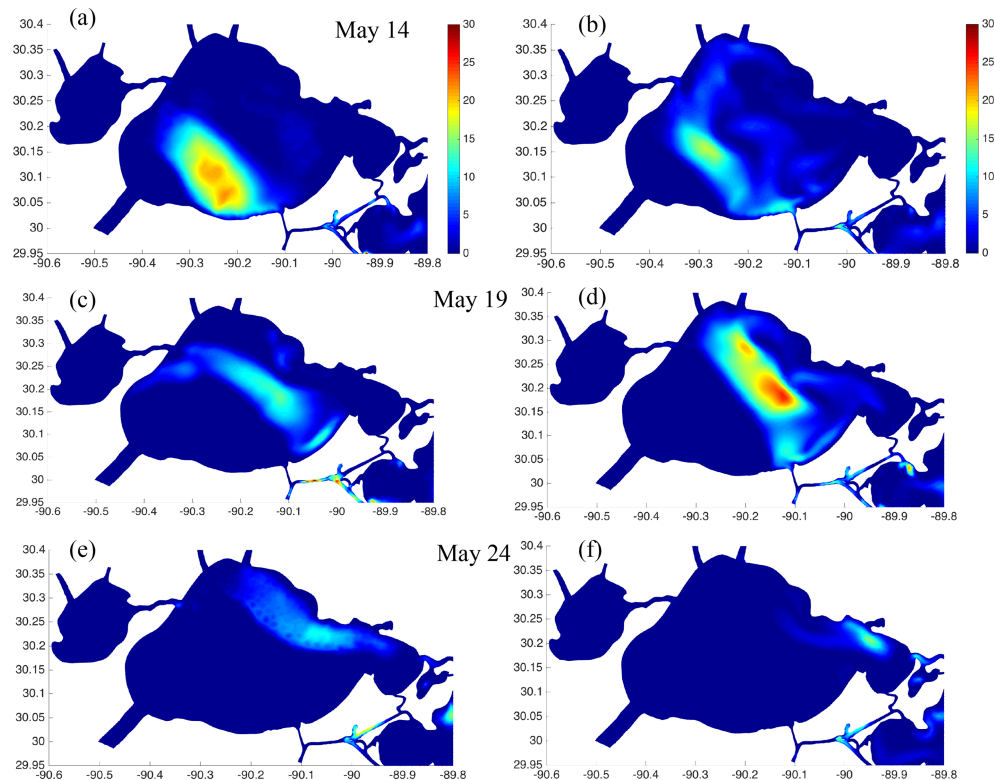


Figure 13. APED contour plot during three cold front events. Figures a, c, and e are results from Experiment 1, Figures b, d, and f are calculated using Experiment 2.

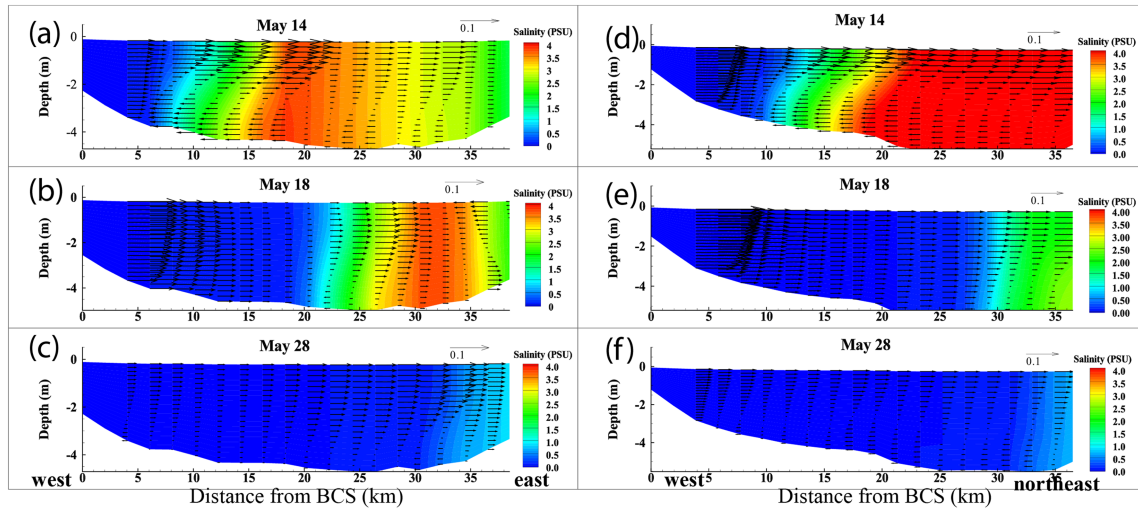


Figure 14. Vertical structure of salinity and along-line velocity for nodes along line 1 (a–c) and line 2 (d–f) on different dates.

where $\partial\zeta$ is the subtidal surface level difference in two directions, ∂x is the cross- and along-estuary distance (37 or 52 km, respectively). Four points from N, S, W, and E sites around the lake are selected. In equation 14, ρ is the water density ($1,024 \text{ kg/m}^3$), h is the average water depth of 4.0 m. τ_{ax} is the wind stress in the cross or along-estuary direction (Garvine, 1985):

$$\tau_{ax} = \rho_a C_d |W| W_x, \quad (15)$$

where ρ_a is the air density (1.29 kg/m^3), C_d is the wind drag coefficient of 1.24×10^{-3} , W_x is the wind velocity component in the cross- or along-estuary direction with a total wind speed of W obtained from the NOAA's National Data Buoy Center station NWCL1 (Figure 1). Quasi-steady state balance induced water level difference resulted from equation 14 is shown in Figure 15 (purple lines).

Water level difference in the along- and cross-estuary directions in the three different experiments are calculated: The first one is from Experiment 1 (blue line in Figure 15); the second one is from Experiment 4 (yellow lines in Figure 15); and the third one from Experiment 3 (red lines in Figure 15). R^2 values between water level differences from equation 14 and that from FVCOM experiments are calculated. R^2 is the highest when there is no diversion nor leakage (0.96 in N-S direction and 0.92 in E-W direction); on the other hand, the R^2 drops to 0.94 and 0.85 in N-S and E-W directions, respectively, after adding the diversion and leakage. Figure 15 reveals that from 8 to 25 May, the discrepancy between the quasi-steady state balance-induced water level difference and that from FVCOM are the largest. This is the time period when a large amount of freshwater is diverted into the lake, apparently interrupting the quasi-steady state balance, demonstrated by a lower R^2 value especially in east-west direction.

5. Discussion: Influence Time of Freshwater Diversion

To quantify the time scale of river diversion effect to reach a given location, we define the influence time of a given node to be the time between the onset of the diversion till the salinity decrease to 0 at that node. This quantity is shown in Figure 16. Obviously, the further away from the diversion, the longer time it takes to be affected by the river water (Figure 16a). However, when there is no wind forcing (Figure 16b), it takes shorter time for the western and northern regions to be influenced by the river diversion and longer for southeastern region to be influenced. This indicates the important role of wind on the evolution of river plume from BCS. In addition, the time for the whole lake to respond to the river plume is about 25 days; that means that the river water is full of freshwater after 25 days (red color in Figure 16a), which is consistent with Figure 5, which shows that the salt content reached its minimum after 5 June. During the diversion, we measured the total discharge at the entrance to the lake using a boat mounted ADCP to be $\sim 6,000\text{--}7,000 \text{ m}^3/\text{s}$. Taking the volume of the lake as $9.77 \times 10^9 \text{ m}^3$, if the freshwater replaces the estuarine water continuously

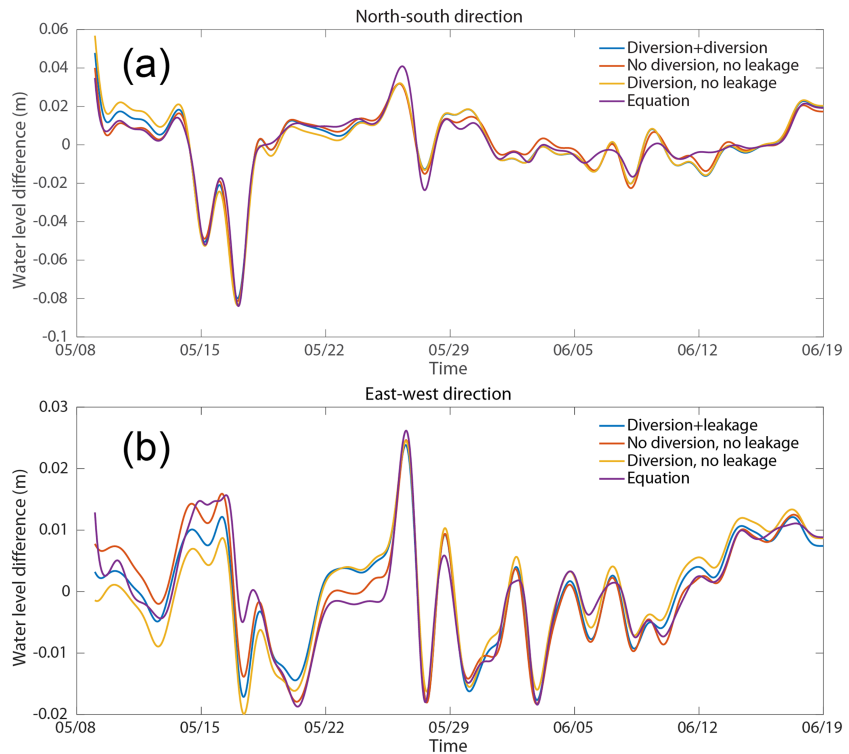


Figure 15. Water level difference from quasi-steady state balance (purple lines) and from FVCOM results (blue line from Experiment 1, red line from Experiment 3, and yellow line from Experiment 4). (a) Water level difference in (a) north-south direction and (b) east-west direction.

at the given rate, it would take about 16–19 days for the entire lake to be filled by freshwater, which is the same order of magnitude as the 25 day influencing time for the whole lake.

An open-source package, the FVCOM I-state Configuration Model (FISCM, 2013) is employed for the Lagrangian particle tracking with 247 freshwater parcels from the BCS. This offline tracking model shows good performance on tracking bay scallops in Buzzards Bay using the results from FVCOM model (Liu et al., 2015). The advection of each individual particle is determined by

$$\frac{d\vec{X}}{dt}(\vec{X}(t), t) = \vec{V}(\vec{X}(t), t), \quad (16)$$

where $\vec{X}(t)$ is the position of the individual particle at time t , \vec{V} is the velocity field resulted from FVCOM. Figure 16c shows the positions after 5, 15, and 20 days, and the ending time of individual particles with the initial positions all at the BCS. Within 10 days (sky blue dots and blue dots in Figure 16c), most of the particles are moving in front of the plume so the positions are in line with the edge of the plume as shown in Figure 3c. After 15 days of opening of the spillway (black dots in Figure 16c), a large number of particles reach the northern shore, and a small portion of the particles are outside of the lake already. On 30 September 2011, 3 months after the opening (red dots in Figure 16c), the particles are randomly distributed on the eastern side of the lake.

When wind forcing is excluded, the only forcing is tide (Figure 16d), the particles are moving toward the southeastern end of the lake and exit the lake through Industrial Canal and Chef Menteur after 15 days of the opening of the spillway. This is due to the Coriolis force making the particles to stay on the right-hand side facing their moving direction.

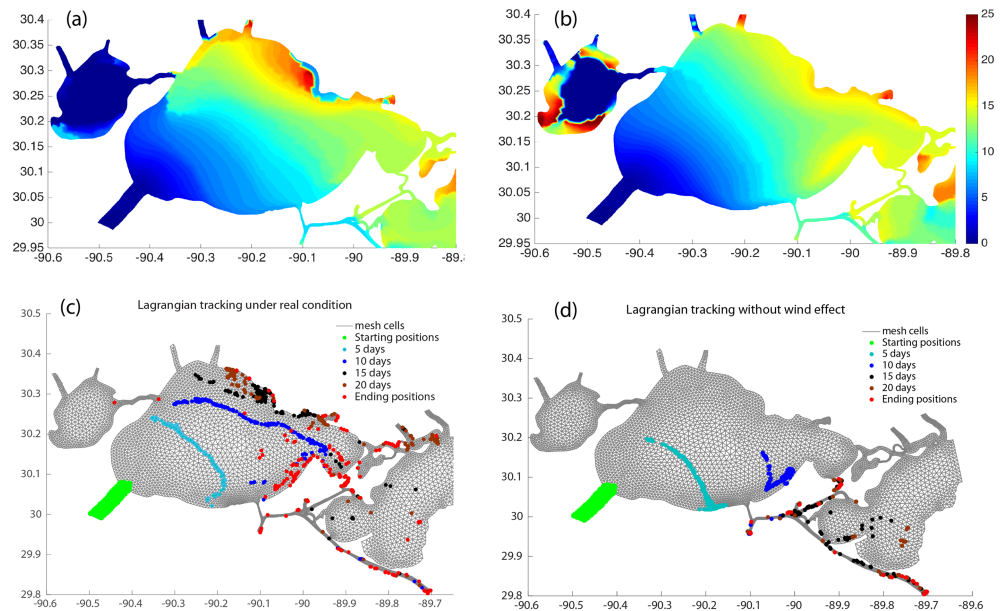


Figure 16. Upper panel is the time for each node being influenced by the freshwater diversion. (a) The case under real condition (Experiment 1). (b) Without wind forcing (Experiment 2). Lower panel is the Lagrangian tracking with (c) and without (d) effect of wind.

6. Summary

The freshwater plume resulted from the opening of the BCS from 9 May to 19 June 2011 is simulated using the hydrodynamic Model FVCOM. FVCOM shows very good performance in simulating the salinity with a skill score of 0.64. The simulated shape of the plume is consistent with that obtained from the satellite images. This work is therefore applicable to tracking the trajectory of the plume nutrient load resulting from river water introduction, and therefore, it may be useful future studies in predicting the potential for algal blooms along the frontal boundary.

The shape of the plume is mainly affected by the location of the BCS, the flow rate and direction and the wind forcing. Southerly wind tends to constrain the expansion of the southeastern edge of the plume. Northerly wind tends to prevent the northeastern edge of the plume from expanding. The shape of the plume is more sensitive to easterly and westerly winds, which tend to limit the edge of the plume extension to the northern shore and stretches the western edge further to the eastern area.

Increasing wind magnitude tends to increase the total salt content inside the system under easterly, northerly, and southerly wind directions. Salt content decreases when wind magnitude changes from 2 to 6 m/s during westerly wind. However, the plume increases when the wind magnitude is larger than 6 m/s, indicating that under westerly wind, when the wind magnitude is smaller than 6 m/s, the rate of the freshwater transported into the estuary from the BCS is larger than that of the saltwater from the eastern open boundary. When the wind continues to increase, the rate of the saltwater transported to the estuary exceeds that of the freshwater transported into the lake, indicating a stronger bottom upwind flow at the open boundary.

A two-layered flow structure (downwind and upwind) can be seen from the model results under various wind conditions, similar to the barotropic cases (Li et al., 2018a). When the magnitude of the wind increases, both surface downwind and bottom upwind flows increase. However, bottom upwind flows tend to be stronger than the surface downwind flow, especially in the central region. Along the coast, the predominant flows tend to be downwind, as in the barotropic cases (Li et al., 2018a). Because of the two-layered structure, there is a no-motion plane between the upwind and downwind flows, which migrates to a lower layer when wind magnitude increases. Water with higher salinity is constrained to further eastern area under westerly wind and extends to further interior under easterly wind. On the other hand, saltier water extends to further northern area under southerly wind. This control of the wind on plume movement can determine the amount of nutrients retained in the system versus the load that leaves the estuary to the coastal ocean and consequently changes the water quality and ecosystem health.

Leakage of river through BCS during flooding season has significant impact on hydrodynamics of the water in the Lake Pontchartrain. The leakage of freshwater reduces nearly 3.7×10^8 kg of salt content of the estuary during the BCS opening period, leading to a drop of 3–4 psu of salinity compared with the condition without the leakage effect. Leakage of freshwater leads to a tendency of diminishing gyres in the lake but increases the mixing of the water, resulting in a very low APED for the whole lake. In addition, together with the influence of diversion, leakage from BCS tends to have an impact on the quasi-steady state balance. Thus, the R^2 between the water level difference from quasi-steady state balance and that from the FVCOM result with freshwater diversion and leakage effect is the lowest in both east-west and north-south directions. The R^2 value however is still above 0.8 and the quasi-steady state balance still holds—the modeled water level gradient still follows the trend of the simple quasi-steady state balance predicted curve over time. The slight departure from the theoretical curve is a result of additional surface slope caused by the freshwater discharge from the diversion, very much similar to the effect of tidally induced mean slope (Li and O'Donnell, 1997) that reduces the R^2 value of the quasi-steady state balance as discussed in Huang and Li (2019).

It takes about 25 days for the whole lake to be influenced by the river diversion from a river spillway opening. Salt content drops from 600,000 kg to less than 100,000 kg after 25 days of the opening of the spillway indicating a significant and sustained freshening effect. This conclusion is consistent with the trajectory of the particles calculated by the Lagrangian tracking.

Acknowledgments

The research was supported by NSF (OCE-1736713, OCE-0554674, DEB-0833225, OCE-1140307, and EAR-1139997), and NOAA (NA06OAR4320264-06111039) through the Northern Gulf Institute by NOAA's Office of Ocean and Atmospheric Research. Our computation using the FVCOM was performed on the cluster computer of the Louisiana Optical Network Initiative (LONI) HPC systems at LSU. Wind data are obtained from NOAA (https://www.ndbc.noaa.gov/station_history.php?station=ncw11; <https://tidesandcurrents.noaa.gov/stationhome.html?id=8761305>; <https://tidesandcurrents.noaa.gov/stationhome.html?id=8747437>). Satellite image from Earth Scan Laboratory of LSU. The USGS river discharge, water level, salinity, and weather data are public domain data. The plume CT data can be accessed from <https://works.bepress.com/Estuary/1/>, and the ADCP data from <https://works.bepress.com/Estuary/2/>. The data are under the Attribution 4.0 International (CC BY 4.0) license for maximum dissemination. The data can also be accessed from a another depository: https://digitalcommons.lsu.edu/oceanography_coastal_wavcis/1/.

References

- Ackerman, D., & Weisberg, S. B. (2003). Relationship between rainfall and beach bacterial concentrations on Santa Monica Bay beaches. *Journal of Water and Health*, *1*, 85–89.
- Allen, J. I., Somerfield, P. J., & Gilbert, F. J. (2007). Quantifying uncertainty in high-resolution coupled hydrodynamic-ecosystem models. *Journal of Marine Systems*, *64*, 3–14. <https://doi.org/10.1016/j.jmarsys.2006.02.010>
- Allison, M. A., Vosburg, B. M., Ramirez, M. T., & Meselhe, E. A. (2013). Mississippi River channel response to the Bonnet Carré Spillway opening in the 2011 flood and its implications for the design and operation of river diversions. *Journal of Hydrology*, *477*, 104–118.
- Androulidakis, Y. S., Kourafalou, V. H., & Schiller, R. Y. (2015). Process studies on the evolution of the Mississippi River plume: Impact of topography, wind and discharge conditions. *Continental Shelf Research*, *107*, 33–49.
- Araújo, C. A. S., Sampiao, F. G., Alcântara, E., Curtarelli, M. P., Ogashawara, I., & Stech, J. L. (2017). Effects of atmospheric cold fronts on stratification and water quality of a tropical reservoir implications for aquaculture. *Aquaculture Environment Interactions*, *9*, 385–403.
- Bargu, S., White, J. R., Li, C., Czubakowski, J., & Fulweiler, R. W. (2011). Effects of freshwater input on nutrient loading, phytoplankton biomass, and cyanotoxin production in an oligohaline estuarine lake. *Hydrobiologia*, *661*, 377–389. <https://doi.org/10.1007/s10750-010-0545-8>
- Berdeal, I. G., Hickey, B. M., & Kawase, M. (2002). Influence of wind stress and ambient flow on a high discharge river plume. *Journal of Geophysical Research*, *107*(C9), 3130. <https://doi.org/10.1029/2001JC000932>
- Chao, S. Y. (1988). River-forced estuarine plume. *Journal of Physical Oceanography*, *18*, 72–88.
- Chao, S. Y., & Boicourt, W. C. (1986). Onset of estuarine plumes. *Journal of Physical Oceanography*, *16*, 2137–2149.
- Chao, X. B., Jia, Y. F., & Azad Hossain, A. K. M. (2013). Numerical modeling of flow and sediment transport in Lake Pontchartrain due to flood release from Bonnet Carré Spillway, sediment transport processes and their modelling applications, Dr. Andrew Manning (Ed.), InTech. <https://doi.org/10.5772/54435>
- Chao, X. B., Jia, Y. F., & Azad Hossain, A. K. M. (2016). Numerical modeling of sediment transport and its effect on algal biomass distribution in Lake Pontchartrain due to flood release from Bonnet Carré Spillway. *Journal of Geoscience and Environment Protection*, *4*, 64–79. <https://doi.org/10.4236/gep.2016.49006>
- Chen, C., Liu, H., & Beardsley, R. C. (2003). An unstructured grid, finite-volume, three dimensional, primitive equation ocean model: Application to coastal ocean and estuaries. *Journal of Atmospheric and Oceanic Technology*, *20*, 159–186.
- Chen, C.-C., Shiah, F.-K., Chiang, K.-P., Gong, G.-C., & Kemp, W. M. (2009). Effects of the Changjiang (Yangtze) River discharge on plankton community respiration in the East China Sea. *Journal of Geophysical Research*, *114*, C03005. <https://doi.org/10.1029/2008JC004891>
- Chen, S.-N., & Sanford, L. (2009). Axial wind effects stratification and longitudinal salt transport in an idealized, partially mixed estuary. *Journal of Physical Oceanography*, *39*, 1905–1920.
- Chilmakuri, C. (2005). *Sediment transport and pathogen indicator modeling in Lake Pontchartrain* (p. 144). New Orleans, Louisiana: University of New Orleans, Doctoral thesis.
- DiGiacomo, P., Washburn, L., Holt, B., & Jones, B. (2004). Coastal pollution hazards in southern California observed by SAR imagery: Stormwater plumes, wastewater plumes, and natural hydrocarbon seeps. *Marine Pollution Bulletin*, *49*(11-12), 1013–1024. <https://doi.org/10.1016/j.marpolbul.2004.07.016>
- Dinnel, S. P., Schroeder, W. W., & Wiseman, W. J. Jr. (1990). Estuarine-shelf exchange using Landsat images of discharge plumes. In *Journal of Coastal Research* (Vol. 6(4), pp. 789–799). Fort: Lauderdale (Florida). ISSN 0749-0208
- Dong, L., Su, J., Wong, L. A., Cao, Z., & Chen, J.-C. (2004). Seasonal variation and dynamics of the Pearl River plume. *Continental Shelf Research*, *24*, 1761–1777.
- Eisma, D. (1981). Suspended matter as a carrier for pollutants in estuaries and the sea. In R. A. Greyer (Ed.), *Marine Environmental Pollution, Elsevier Oceanogr. Ser* (Vol. 27, pp. 281–295). Amsterdam.
- Engelund, F. (1973). In F. B. Pedersen (Ed.), *Steady wind set-up in prismatic lakes, reprinted in environmental hydraulics: Stratified flows (lecture notes on coastal and estuarine studies, vol. 18)* (Vol. 1986, pp. 205–212). New York: Springer.
- FISCM (2013). FVCOM I-State Configuration Model (FISCM) source code. Retrieved from <http://github.com/GeoffCowles/fiscm>

- Fong, D. A., & Geyer, W. R. (2001). Response of a river plume during an upwelling favorable wind event. *Journal of Geophysical Research*, *106*(C1), 1067–1084.
- Fong, D. A., & Geyer, W. R. (2002). The alongshore transport of freshwater in a surface-trapped river plume. *Journal of Physical Oceanography*, *32*, 957–972.
- Galperin, B., Kantha, L. H., Hassid, S., & Rosati, A. (1988). A quasi-equilibrium turbulent energy model for geophysical flows. *Journal of the Atmospheric Sciences*, *45*, 55–62.
- Gan, J., Li, L., Wang, D., & Guo, X. (2009). Interaction of a river plume with coastal upwelling in the northeastern South China Sea. *Continental Shelf Research*, *29*, 728–740.
- Garvine, R. (1977). Observations of the motion filed of the Connecticut Rive plume. *Journal of Geophysical Research*, *82*(3), 441–454.
- Garvine, R. (1987). Estuary plumes and fronts in shelf waters: A layer model. *Journal of Physical Oceanography*, *17*, 1877–1896.
- Garvine, R., & Monk, J. D. (1974). Frontal structure of a river plume. *Journal of Geophysical Research*, *79*(15), 2521–2529.
- Garvine, R. W. (1984). Radial spread of buoyant surface plumes in coastal waters. *Journal of Geophysical Research*, *89*, 1989–1996.
- Garvine, R. W. (1985). A simple model of estuarine subtidal fluctuations forced by local and remote wind stress. *Journal of Geophysical Research*, *90*(C6), 11,945–11,948. <https://doi.org/10.1029/JC090iC06p11945>
- Georgiou, I. Y., Retana, A. G., McCorquodale, J. A., Schindler, J., Fitzgerald, D. M., Hughes, Z., & Howes, N. (2009). Impact of multiple freshwater diversions on the salinity distribution in the Pontchartrain Estuary under tidal forcing. *Journal of Coastal Research*, *SI*(54), 59–70. West Palm Beach (Florida), ISSN 0749-0208
- Halverson, M. J., & Pawlowicz, R. (2008). Estuarine forcing of a river plume by river flow and tides. *Journal of Geophysical Research*, *113*, C09033. <https://doi.org/10.1029/2008JC004844>
- Hickey, B. M., Pietrafesa, L. J., Day, D. A., & Bouicourt, W. C. (1998). The Columbia River plume study: Subtidal variability in the velocity and salinity fields. *Journal of Geophysical Research*, *103*, 10,339–10,368.
- Hordoir, R., Nguyen, K. D., & Polcher, J. (2006). Simulating tropical river plumes, a set of parametrizations based on macroscale data: A test case in the Mekong Delta region. *Journal of Geophysical Research*, *111*, C09036. <https://doi.org/10.1029/2005JC003392>
- Horner-Devine, A. R. (2009). The bulge circulation in the Columbia River plume. *Continental Shelf Research*, *29*, 234–251.
- Horner-Devine, A. R., Jay, D. A., Orton, P. M., & Spahn, E. Y. (2009). A conceptual model of the strongly tidal Columbia River plume. *Journal of Marine Systems*, *78*, 460–475.
- Houghton, R. W., Tilburg, C. E., Garvine, R. W., & Fong, A. (2004). Delaware River plume response to a strong upwelling-favorable wind event. *Geophysical Research Letters*, *31*, L07302. <https://doi.org/10.1029/2003GL018988>
- Huang, W., & Li, C. (2017). Cold front driven flows through multiple inlets of Lake Pontchartrain Estuary. *Journal of Geophysical Research*, *122*, 8627–8645.
- Huang, W., & Li, C. (2019). Spatial variation of cold front wind-driven circulation and quasi-steady state balance in Lake Pontchartrain Estuary. *Estuarine, Coastal and Shelf Science*, *224*, 154–170.
- Huang, W.-J., Cai, W.-J., Castelao, R. M., Wang, W., & Lohrenz, S. E. (2013). Effects of a wind-driven cross-shelf large river plume on biological production and CO₂ uptake on the Gulf of Mexico during spring. *Limnology and Oceanography*, *58*(5), 1727–1735. <https://doi.org/10.4319/lo.2013.58.5.1727>
- Jiang, L., Yan, X.-F., & Klemas, V. (2009). Remote sensing for the identification of coastal plumes: Case studies of Delaware Bay. *International Journal of Remote Sensing*, *30*(8), 2033–2048.
- Kakoulaki, G., McDonald, D., & Horner-Devine, A. R. (2014). The role of wind in the near field and midfield of a river plume. *Geophysical Research Letters*, *41*, 5132–5138. <https://doi.org/10.1002/2014GL060606>
- Keddy, P. A., Campbell, D., McFalls, T., Shaffer, G., Moreau, R., Dranguet, C., & Heleniak, R. (2007). The wetlands of lakes Pontchartrain and Maurepas: Past, present and future. *Environmental Reviews*, *15*, 1–35. Table 2
- Kourafalou, V. H., Oey, L.-Y., Wang, J. D., & Lee, T. N. (1996). The fate of river discharge on the continental shelf 1. Modeling the river plume and the inner shelf coastal current. *Journal of Geophysical Research*, *101*(C2), 3415–3434.
- Lane, R. R., Day, J. W. Jr., Kemp, G. P., & Demcheck, D. K. (2001). The 1994 experimental opening of the Bonnet Carré Spillway to divert Mississippi River water into Lake Pontchartrain, Louisiana. *Ecological Engineering*, *17*, 411–422.
- Large, W. G., & Pond, S. (1981). Open ocean momentum flux measurements in moderate to strong winds. *Journal of Physical Oceanography*, *11*, 324–336.
- Lee, J., & Valle-Levinson, A. (2013). Bathymetric effects on estuarine plume dynamics. *Journal of Geophysical Research*. *Oceans*, *118*, 1969–1981. <https://doi.org/10.1002/jgrc.20119>
- Lehrter, J. C., Murrell, M. C., & Kurtz, J. C. (2009). Interactions between freshwater input, light, and phytoplankton dynamics on the Louisiana continental shelf. *Continental Shelf Research*, *29*, 1861–1872.
- Lentz, S. (1995). The Amazon River plume during AMASSEDSL: Subtidal current variability and the importance of wind forcing. *Journal of Geophysical Research*, *100*(C2), 2377–2390.
- Li, C., Boswell, K. M., Chaichitehrani, N., Huang, W., & Wu, R. (2019). Weather induced subtidal flows through multiple inlets of an Arctic micro-tidal lagoon. *Acta Oceanologica Sinica*, *38*(3), 1–16. <https://doi.org/10.1007/s13131-019-1361-2>
- Li, C., Huang, W., Chen, C., & Lin, H. (2018). Flow regimes and adjustment to wind-driven motions in Lake Pontchartrain: A modeling experiment using FVCOM. *Journal of Geophysical Research*, *Oceans*, *123*(11), 8460–8488. <https://doi.org/10.1029/2018JC013985>
- Li, C., Huang, W., & Milan, B. (2019). Atmospheric cold front induced exchange flows through a microtidal multi-inlet bay: Analysis using multiple horizontal ADCPs and FVCOM simulations. *Journal of Atmospheric and Oceanic Technology*, *36*, 443–472.
- Li, C., Roberts, H., Stone, G., Weeks, E., & Luo, Y. (2011). Wind surge and saltwater intrusion in Atchafalaya Bay under onshore winds prior to cold front passage. *Hydrobiologia*, *658*(1), 27–39. <https://doi.org/10.1007/s10750-010-0467-5>
- Li, C., Walker, N., Hou, A., Georgiou, I., Roberts, H. H., Laws, E., et al. (2008). Circular plumes in Lake Pontchartrain Estuary under wind straining. *Estuarine, Coastal and Shelf Science*, *80*, 161–172.
- Li, C., Weeks, E., Huang, W., Milan, B., & Wu, R. (2018). Weather induced transport through a tidal channel calibrated by an unmanned boat. *Journal of Atmospheric and Oceanic Technology*, *35*(2), 261–279.
- Li, C., Weeks, E., & Rego, J. L. (2009). In situ measurements of saltwater flux through tidal passes of Lake Pontchartrain estuary by Hurricanes Gustav and Ike in September 2008. *Geophysical Research Letters*, *36*, L19609. <https://doi.org/10.1029/2009GL039802>
- Li, Y., & Li, M. (2011). Effects of winds on stratification and circulation in a partially mixed estuary. *Journal of Geophysical Research*, *116*, C12012. <https://doi.org/10.1029/2010JC006893>
- Li, Y., & Li, M. (2012). Wind-driven lateral circulation in a stratified estuary and its effects on the along-channel flow. *Journal of Geophysical Research*, *117*, C09005. <https://doi.org/10.1029/2011C008929>

- Lin, J., Li, C., Boswell, K. M., Kimball, M., & Rozas, L. (2016). Examination of winter circulation in a Northern Gulf of Mexico Estuary. *Estuaries and Coasts*, *39*(4), 879–899. <https://doi.org/10.1007/s12237-015-0048-y>
- Liu, C., Cowles, G. W., Churchill, J. H., & Stokesbury, K. D. E. (2015). Connectivity of the bay scallop (*Argopecten irradians*) in Buzzards Bay, Massachusetts, U.S.A. *Fisheries Oceanography*, *24*(4), 364–382.
- Marsaleix, P., Estournel, C., Kondrachoff, V., & Vehil, R. (1998). A numerical study of the formation of the Rhône River plume. *Journal of Marine Systems*, *14*, 99–115.
- McCorquodale, A. J., Roblin, R. J., Georgiou, I. Y., & Haralampides, K. A. (2009). Salinity, nutrient, and sediment dynamics in the Pontchartrain Estuary. *Journal of Coastal Research*, *SI*(54), 71–87. West Palm Beach (Florida), ISSN 0749-0208
- Mellor, G. L., & Yamada, T. (1982). Development of a turbulence closure model for geophysical fluid problem. *Reviews of Geophysics and Space Physics*, *20*, 851–875.
- Nezlin, N. P., DiGiacomo, P. M., Diehl, D. W., Jones, B. H., Johnson, S. C., Mengel, M. J., et al. (2008). Stormwater plume detection by MODIS imagery in the southern California coastal ocean. *Estuarine, Coastal and Shelf Science*, *80*(1), 141–152. <https://doi.org/10.1016/j.ecss.2008.07.012>
- O'Donnell, J. (1990). The formation and face of a river plume: A numerical model. *Journal of Physical Oceanography*, *20*, 551–569.
- O'Donnell, J., Ackleson, S. G., & Levine, E. R. (2008). On the spatial scales of a river plume. *Journal of Geophysical Research*, *113*, C04017. <https://doi.org/10.1029/2007JC004440>
- O'Donnell, J., Marmorino, G. O., & Trump, C. L. (1998). Convergence and downwelling at a river plume front. *Journal of Physical Oceanography*, *28*, 1481–1495.
- Oey, L.-Y., & Mellor, G. L. (1993). Subtidal variability of estuarine outflow, plume, and coastal current: A model study. *Journal of Physical Oceanography*, *23*, 164–171.
- Ou, S., Zhang, H., & Wang, D.-X. (2009). Dynamics of the buoyant plume off the Pearl River estuary in summer. *Environmental Fluid Mechanism*, *9*, 471–492. <https://doi.org/10.1007/s10652-009-9146-3>
- Retana, A. G. (2008). *Salinity transport in a finite-volume sigma-layer tree dimensional model* (p. 689). New Orleans, Louisiana: University of New Orleans, Doctoral thesis.
- Roy, E. D., Nguyen, N., Bargu, S., & White, J. R. (2012). Internal loading of phosphorus from sediments of Lake Pontchartrain (Louisiana, USA) with Implications for Eutrophication. *Hydrobiologia*, *684*, 69–82.
- Roy, E. D., Smith, E. A., Bargu, S., & White, J. R. (2016). Will Mississippi River diversions designed for coastal restoration cause harmful algal blooms? *Ecological Engineering*, *91*, 350–364.
- Roy, E. D., White, J. R., Smith, E. A., Bargu, S., & Li, C. (2013). Estuarine ecosystem response to three large-scale Mississippi River flood diversion events. *Science of the Total Environment*, *458*, 374–387.
- Shi, W., & Wang, M. (2009). Satellite observations of flood-driven Mississippi River plume in the spring of 2008. *Geophysical Research Letters*, *36*, L07607. <https://doi.org/10.1029/2009GL037210>
- Simpson, J. H., Brown, J., Matthews, J., & Allen, G. (1990). Tidal straining, density currents, and stirring in the control of estuarine stratification. *Estuaries*, *13*(2), 125–132.
- Valle-Levinson, A., Holderied, K., Li, C., & Chant, R. J. (2007). Subtidal flow structure at the turning region of a wide outflow plume. *Journal of Geophysical Research*, *112*, C04004. <https://doi.org/10.1029/2006JC003746>
- van den Huevel, S., 2010. Modeling the hydrodynamics and salinity of the Pontchartrain Basin, Master's Thesis, Delft University of Technology.
- Walker, D. N., Wiseman, W. J. Jr., Rouse, L. J. Jr., & Babin, A. (2005). Effects of river discharge, wind stress, and slope eddies on circulation and the satellite-observed structure of the Mississippi River plume. *Journal of Coastal Research*, *21*(6), 1228–1244. West Palm Beach (Florida), ISSN 0749-0208
- Walker, N. D. (1999). Satellite assessment of Mississippi River plume variability: Cause and predictability. *Remote Sensing of Environment*, *58*, 21–35.
- Walker, N. D., Huh, O. K., Rouse, L. J. Jr., & Murray, S. P. (1996). Evolution and structure of a coastal squirt off the Mississippi River delta: Northern Gulf of Mexico. *Journal of Geophysical Research*, *101*(C9), 20,643–20,655.
- Weeks, E., Robinson, M. E., & Li, C. (2018). Quantifying cold front induced water transport of a bay with *in situ* observations using manned and unmanned boats. *Acta Oceanologica Sinica*, *37*(11), 1–7. <https://doi.org/10.1007/s13131-018-1330-1>
- White, J. R., Fulweiler, R. W., Li, C., Bargu, S., Walker, N. D., Twilley, R. R., & Green, S. E. (2009). Mississippi River flood of 2008: Observations of a large freshwater diversion on physical, chemical, and biological characteristics of shallow estuarine lake. *Environmental Science and Technology*, *43*(15), 5599–5604. <https://doi.org/10.1021/es900318t>
- Wiseman, W. J., & Garvine, R. W. (1995). Plumes and coastal currents near large river mouths. *Estuaries*, *18*(3), 509–517.
- Xie, X., & Li, M. (2018). Effects of wind straining on estuarine stratification: A combined observational and modeling study. *Journal of Geophysical Research, Oceans*, *123*, 2363–2380. <http://doi.org/10.1002/2017JC013470>
- Zheng, S., Guan, W., Cai, S., Wei, X., & Huang, D. (2014). A model study of the effects of river discharges and interannual variation of winds on the plume front in winter in Pearl River Estuary. *Continental Shelf Research*, *73*, 31–40.
- Zu, T., & Gan, J. (2015). A numerical study of couple estuary-shelf circulation around the Pearl River estuary during summer: responses to variable winds, tides and river discharge. *Deep Sea Research, Part II*, *117*, 53–64.
- Zu, T., Wang, D., Gan, J., & Guan, W. (2014). On the role of wind and tide in generating variability of Pearl River plume during summer in a coupled wide estuary and shelf system. *Journal of Marine Systems*, *136*, 65–79.